UNIVERSITY OF OKLAHOMA

GRADUATE COLLEGE

NEAR SURFACE ATMOSPHERIC IMPACTS RESULTING FROM A DEVELOPING METROPOLITAN AREA

A DISSERTATION

SUBMITTED TO THE GRADUATE FACULTY

in partial fulfillment of the requirements for the

Degree of

DOCTOR OF PHILOSOPHY

By

BRADLEY GLEN ILLSTON
Norman, Oklahoma
2016

Downloaded from SHAREOK. Persistent Handle URL: https://hdl.handle.net/11244/47037

NEAR SURFACE ATMOSPHERIC IMPACTS RESULTING FROM A DEVELOPING METROPOLITAN AREA

A DISSERTATION APPROVED FOR THE
SCHOOL OF METEOROLOGY

BY

Dr. Jeffrey B. Basara, Chair

Dr. Petra Klein

Dr. Michael B. Richman

Dr. Xiaoming Hu

Dr. Aondover Tarhule

© Copyright by BRADLEY GLEN ILLSTON 2016
All Rights Reserved.

Acknowledgements

I would like to deeply thank the many people who helped me accomplish this monumental task. It has been a very long road and I have learned a tremendous amount, not only scientifically, but about the supportive people with which I have surrounded myself.

This research could not have been accomplished without the world-class work done by the Oklahoma Mesonet employees. From the technicians working in the field to keep stations running to the operators watching the site communications carefully. From quality assurance meteorologists meticulously analyzing observations to the computer hardware and software engineers working to keep everything running smoothly. The Oklahoma Mesonet is truly a team effort and I am honored to be a part of that team.

A special thank you to the City of Oklahoma City Public Works department for being an integral part of the Oklahoma City Micronet whose data was critical in allowing this research to be what it is.

I would like to thank all of my friends and colleagues for their support and encouragement. From lending an ear to hear me rant about research problems to suggestions on avenues to solve unforeseen issues, they were always there for me.

While many people may overlook the importance of their PhD committee, I never once took for granted the members on my committee. I was honored when each of the members agreed to serve on my committee and guide me through the doctoral processes. My road to completing my doctorate was longer than most, but my committee remained patient and ensured that my path always led me towards completion.

I never can thank enough all that my family has done for me in instilling a strong work ethic and to never settle for less than you desire. At the culmination of my educational career, I have looked back over the years and recollected about all of the times they encouraged me. At times, eyes may have been glazed over when I tried to explain my work, but I realized that those glazed eyes showed me the love and pride that they had for me. Regardless of where the future leads me, I will always remember that "you have only failed when you have failed to try."

Finally, I could not stand as tall and be as proud of myself without all of the support and encouragement from my love, Leslie. At times, it seemed like the world was against us, testing us more than we felt we deserved. But having each other, we have learned how to overcome our tribulations and come out stronger than before. Nothing can stand in our way and our future looks bright. You make me want to be the man that I know I can be.

Table of Contents

Acknowledgements iv

Table of Contents vi

List of Tables viii

List of Figures ix

Abstract xiv

Chapter 1: Introduction 1

Chapter 2: Scientific Background 3

- Population Trends 3
- Urban Meteorological Studies 5
- Urban Atmospheric Modeling 7
- Oklahoma City 8

Chapter 3: Observational Data 11

- Oklahoma Mesonet 11
- Oklahoma City Micronet 11
- Urban Heat Islands 12

Chapter 4: Numerical Urban Modelling System 15

- Candidate Days 15
- The Weather Research and Forecasting (WRF) Model 15
  - Domains 16
  - Input Data / Background Fields 17
  - The Uncoupled High Resolution Land Data Assimilation System: HR-LDAS 19

Chapter 5: Run-time Accuracy 20

- 21 June 2008 Case Study 21
- 1 August 2008 Case Study 22
- 5 September 2008 Case Study 23
- 15 September 2008 Case Study 25
- 15 March 2009 Case Study 26
- Summary 28

Chapter 6: Urban Heat Island Changes Over Time 29

21 June 2008 Case Study 30
1 August 2008 Case Study 31
5 September 2008 Case Study 32
15 September 2008 Case Study 32
15 March 2009 Case Study 33
Summary 34

Chapter 7: Alternate Urban Heat Island Methodologies 35

Verification Siting Issue (Mesonet vs. Selected Rural) 35
Top 10/100/500/1000 Warmest Locations UHII 36
2 m Air Temperature Coverage Percentile Increases 39
2 m Air Temperature Distribution Shift 40

Chapter 8: Conclusions 43

References 47

Appendix A: Tables 55

Appendix B: Figures 60

List of Tables

Table 1. A list of candidate days indicating their season and their meteorological conditions at 12 UTC. Urban/Rural temperatures are an average of the temperatures measured from Oklahoma City Micronet Central Business District stations (e.g. urban) and Oklahoma Mesonet stations surrounding the Oklahoma City area (e.g. "rural"). The urban heat island index is the difference between the urban and rural averaged temperatures. 55

Table 2. A list of WRF/WPS options selected for all model runs. 56

Table 3. Mean errors in air temperature in model simulations of 02 UTC ("Validation Time"), 01-03 UTC ("±1 hr"), and the 18 hours ending at 12 UTC ("All Times") for the 21 June 2008 case. 57

Table 4. Mean errors in air temperature in model simulations of 06 UTC ("Validation Time"), 05-07 UTC ("±1 hr"), and the 18 hours ending at 12 UTC ("All Times") for the 1 August 2008 case. 57

Table 5. Mean errors in air temperature in model simulations of 02 UTC ("Validation Time"), 01-03 UTC ("±1 hr"), and the 18 hours ending at 12 UTC ("All Times") for the 5 September 2008 case. 58

Table 6. Mean errors in air temperature in model simulations of 02 UTC ("Validation Time"), 01-03 UTC ("±1 hr"), and the 18 hours ending at 12 UTC ("All Times") for the 15 September 2008 case. 58

Table 7. Mean errors in air temperature in model simulations of 03 UTC ("Validation Time"), 02-04 UTC ("±1 hr"), and the 18 hours ending at 12 UTC ("All Times") for the 15 March 2009 case. 59

List of Figures

Figure 1. Methodology flow chart of this research study indicating procedures and results of original content and results. 60

Figure 2. Urban and rural population trends and projections of the world. (United Nations, 2009)..... 61

Figure 3. Urban and rural population trends and projections of the United States. (United Nations, 2009) 61

Figure 4. Topographical map of Oklahoma. (Courtesy of Oklahoma Mesonet)..... 61

Figure 5. A map of the Oklahoma Mesonet in 2010. 61

Figure 6. A map of the Oklahoma City Micronet with a Central Business District inset. 61

Figure 7. Mean diurnal air temperature gradients between 2 m and 9 m in urban and rural locations during Joint Urban 2003. (Basara et al., 2008) 61

Figure 8. Example of a heat island measured by the Oklahoma City Micronet. (Schroeder et al., 2010). 61

Figure 9. WRF domains: 4050 km x 4050 km with 40.5 km grid spacing (d01), 1350 km x 1350 km with 13.5 km grid spacing (d02), 450 km x 450 km with 4.5 km grid spacing (d03), 150 km x 150 km with 1.5 km grid spacing (d04), and 50 km x 50 km with 500 m grid spacing (d05). 61

Figure 10. Historical information with which the background land cover images for 1890 were created. 61

Figure 11. Historical information with which the background land cover images for 1920 were created. 61

Figure 12. Historical information with which the background land cover images for 1950 were created. 61
Figure 13. Historical information with which the background land cover images for 1980 were created. 61
Figure 14. Historical information with which the background land cover images for 2011 were created. 61
Figure 15. WRF initialization field of soil moisture conditions at a 1-km grid using just NARR initial conditions and no NLDAS spin-up (left) and using a 5-year spin up of NLDAS and NARR initial conditions (right). (Nemunaitis, 2014)..... 61
Figure 16. Run time accuracy of air temperature simulations at 2 m for urban stations (a), rural stations (b), and the resulting UHII (c) for 21 June 2008 case study. The simulation comparison of historical 24 hour UHII simulations (d) are also shown..... 61
Figure 17. Run time accuracy of air temperature simulations at 2 m for urban stations (a), rural stations (b), and the resulting UHII (c) for 1 August 2008 case study. The simulation comparison of historical 24 hour UHII simulations (d) are also shown..... 61
Figure 18. Run time accuracy of air temperature simulations at 2 m for urban stations (a), rural stations (b), and the resulting UHII (c) for 5 September 2008 case study. The simulation comparison of historical 24 hour UHII simulations (d) are also shown..... 61
Figure 19. Run time accuracy of air temperature simulations at 2 m for urban stations (a), rural stations (b), and the resulting UHII (c) for 15 September 2008 case study. The simulation comparison of historical 24 hour UHII simulations (d) are also shown..... 61

Figure 20. Run time accuracy of air temperature simulations at 2 m for urban stations (a), rural stations (b), and the resulting UHII (c) for 15 March 2009 case study. The simulation comparison of historical 24 hour UHII simulations (d) are also shown..... 61
Figure 21. Air temperature at 2 m at 02 UTC from 1890, 1920, 1950, 1980, and 2011 for the 21 June 2008 case study. 61
Figure 22. Air temperature difference at 2 m at 02 UTC from the 1890 land use model run for 1920, 1950, 1980, and 2011 for the 21 June 2008 case study. 61
Figure 23. Air temperature at 2 m at 06 UTC from 1890, 1920, 1950, 1980, and 2011 for the 1 August 2008 case study. 61
Figure 24. Air temperature difference at 2 m at 06 UTC from the 1890 land use model run for 1920, 1950, 1980, and 2011 for the 1 August 2008 case study. 61
Figure 25. Air temperature at 2 m at 02 UTC from 1890, 1920, 1950, 1980, and 2011 for the 5 September 2008 case study. 61
Figure 26. Air temperature difference at 2 m at 02 UTC from the 1890 land use model run for 1920, 1950, 1980, and 2011 for the 5 September 2008 case study. 61
Figure 27. Air temperature at 2 m at 02 UTC from 1890, 1920, 1950, 1980, and 2011 for the 15 September 2008 case study. 61
Figure 28. Air temperature difference at 2 m at 02 UTC from the 1890 land use model run for 1920, 1950, 1980, and 2011 for the 15 September 2008 case study. 61
Figure 29. Air temperature at 2 m at 03 UTC from 1890, 1920, 1950, 1980, and 2011 for the 15 March 2009 case study. 61
Figure 30. Air temperature difference at 2 m at 03 UTC from the 1890 land use model run for 1920, 1950, 1980, and 2011 for the 15 March 2009 case study. 61

Figure 31. Urban and rural air temperatures (a; “Urban”, “Rural”) and Urban heat island indices (b; “UHII”) for arbitrary locations for the top 10, 100, 500, and 1000 warmest grid box locations in the 21 June 2008 at 02 UTC case study. 61
Figure 32. Urban and rural air temperatures (a; “Urban”, “Rural”) and Urban heat island indices (b; “UHII”) for arbitrary locations for the top 10, 100, 500, and 1000 warmest grid box locations in the 1 August 2008 at 06 UTC case study. 61
Figure 33. Urban and rural air temperatures (a; “Urban”, “Rural”) and Urban heat island indices (b; “UHII”) for arbitrary locations for the top 10, 100, 500, and 1000 warmest grid box locations in the 5 September 2008 at 02 UTC case study..... 61
Figure 34. Urban and rural air temperatures (a; “Urban”, “Rural”) and Urban heat island indices (b; “UHII”) for arbitrary locations for the top 10, 100, 500, and 1000 warmest grid box locations in the 15 September 2008 at 02 UTC case study..... 61
Figure 35. Urban and rural air temperatures (a; “Urban”, “Rural”) and Urban heat island indices (b; “UHII”) for arbitrary locations for the top 10, 100, 500, and 1000 warmest grid box locations in the 15 March 2009 at 03 UTC case study. 61
Figure 36. Air temperature coverage percentile increases in the 21 June 2008 at 02 UTC case study..... 61
Figure 37. Air temperature coverage percentile increases in the 1 August 2008 at 03 UTC case study..... 61
Figure 38. Air temperature coverage percentile increases in the 5 September 2008 at 02 UTC case study..... 61
Figure 39. Air temperature coverage percentile increases in the 15 September 2008 at 02 UTC case study..... 61

Figure 40. Air temperature coverage percentile increases in the 15 March 2009 at 03 UTC case study..... 61
Figure 41. Histogram of air temperatures at 2 m at 02 UTC (a), for the daily maximum (b), and for the daily minimum (c) for the 21 June 2008 case study..... 61
Figure 42. Histogram of air temperatures at 2 m at 06 UTC (a), for the daily maximum (b), and for the daily minimum (c) for the 1 August 2008 case study. 61
Figure 43. Histogram of air temperatures at 2 m at 02 UTC (a), for the daily maximum (b), and for the daily minimum (c) for the 5 September 2008 case study. 61
Figure 44. Histogram of air temperatures at 2 m at 02 UTC (a), for the daily maximum (b), and for the daily minimum (c) for the 15 September 2008 case study. 61
Figure 45. Histogram of air temperatures at 2 m at 03 UTC (a), for the daily maximum (b), and for the daily minimum (c) for the 15 March 2009 case study..... 61

Abstract

Over the past century, the population of the world has become increasingly urbanized. As a result, cities have become larger and more densely populated than any time in history. This unprecedented growth and rapid modification of the surface has impacted the overlying boundary-layer of the atmosphere. As such, understanding the overall magnitude and spatial variability of these changes has critical value to the ever growing population living within the impacted regions. The goal of this study is to determine the impact of urbanization on near surface atmospheric conditions and how those impacts evolve with time.

The Weather Research & Forecasting (WRF) model was utilized to simulate atmospheric conditions in and around the Oklahoma City area. The WRF output was compared to surface observations from the Oklahoma City Micronet and the Oklahoma Mesonet to quantify model accuracies and biases. The National Land Cover Dataset (NLCD) was subsequently modified to represent land use characteristics from 1890, following the Oklahoma Land Rush, to 2011 at intervals of every 30 years. The WRF model was initialized with modified NLCD land use datasets to determine the impact from a developing metropolitan area.

An analysis of the optimal simulation run times demonstrated that the 24-hour run time provided the most accurate results in the variety of scenarios and the urban heat island index was within about 0.5°C of the verification from surface observing stations. The results yielded an increase in urban heat island indices of over 3.5°C throughout the past 120 years with an over 5.0°C magnitude warming of the near surface air temperatures over and around the developed urban areas. The analysis of the 1890 land use background

showed that the natural variability of air temperatures without any influences from the metropolitan area are on the order of 1-2°C.

Additionally, implementing unique methodologies for interpreting urban heat characteristics demonstrated that by utilizing the top 10, 100, 500, and 1000 warmest model simulation pixels as urban values instead of arbitrary points, a more representative value for urban heat island indices was calculated (resulting in a value of about 3.5°C in the summer in 2011). The use of air temperature histograms (in particular for the minimum temperature) of the model grid point's output showed changes in the historical distribution of air temperature values indicating a transition towards warmer values over time. Additionally, an analysis of the distribution of air temperature values across the entire domain for each of the historical time periods showed the areal spread of air temperature impacts by over 20%.

Chapter 1: Introduction

Over the past century, the population of the world has become increasingly any time in history (Cohen, 2005). This unprecedented growth and rapid modification of the surface has impacted the overlying boundary-layer of the atmosphere. As such, understanding the overall magnitude and spatial variability of these changes has critical value to the ever-growing population living within the impacted regions.

The hypothesis of this study is that the anthropogenic urbanization in and around Oklahoma City has led to noticeable impacts in the near-surface meteorological conditions. To test this hypothesis, the following questions will be addressed:

1. What run-time length of the Weather Research and Forecasting (WRF) model produces the results with the lowest differences to measured observations?
2. How has the urbanization of Oklahoma City impacted atmospheric conditions since the city was founded in 1890?
3. What are the characteristics of the atmospheric conditions generated by the WRF model over Oklahoma City during urban heat island events?
4. What statistical methods can be utilized to best describe urban heat island events from gridded model output data?

For the first time, a comprehensive analysis of historical urban growth impacts towards urban heat island characteristics and additional statistical methodologies to quantify urban heat severity will be presented (Fig. 1). The goal of this study is to determine the impact of urbanization on near surface atmospheric conditions and how

those impacts evolve with time. The results of this work will have technical merit to the science of meteorology: (1) through improved understanding of mesoscale and urban climate quantified using numerical weather prediction, and (2) there remains a scientific need for the understanding of the temporal scales of mesoscale numerical modeling needed to resolve accurate urban meteorological signals. This research will also impact the broader community through a better understanding of the spatial impacts of near surface meteorological conditions from the development of a metropolitan area in which the general public live and work. As more people move into urban areas and cities become larger, the impact of urban meteorological conditions on life (e.g. higher urban temperatures leading to death, weaker winds leading to trapped aerosols and lung diseases, etc.) are of a higher concern to public safety and this research will aid in a better understanding of potential conditions for growing, existing, and future cities. Similarly, city planners of metropolitan areas could greatly benefit their understating of future impacts by utilizing the knowledge of how different types of urbanizations could impact the atmosphere.

Chapter 2: Scientific Background

Population Trends

Over the past 2000 years, the world has rapidly become more urbanized, a process which has accelerated greatly in the 20th century. As of 2008, the population of the globe was 6.3 million people and growing at a rate of approximately 1.2 percent, 75 million people per year, or 200,000 people per day (United Nations, 2000; US Census Bureau, 2004; Cohen, 2005; Lee, 2009). Most of this growth is in the urban environment (United Nations Human Settlements Program, 1997; Dabberdt et al., 2000; United Nations, 2003; Lee, 2009) as the world's rural population has remained at approximately 3 billion people (Cohen, 2003; Cohen, 2005). In 2007 and for the first time in history, more people lived in urban areas than in rural areas. Figure 2 shows the past and future global projection of population.

Cohen (2003) noted that issues relating to this population growth are critical as "the human species lacks any prior experience with such rapid growth and large numbers of its own species". The 20th century yielded the highest population growth rate in history (2.1% in 1965) and is the only century in which the global population not only doubled, but tripled (Cohen, 2003; Cohen, 2005). While the population growth rate has weakened and is projected to decline, population growth models are still uncertain of the future population totals (United Nations, 2000). The consensus estimation of future worldwide population is 8.9 to 9.1 billion people will inhabit the planet in 2050 with estimates ranging between 7.3 and 11.7 billion (United Nations, 2000; Cohen, 2003; Cohen, 2005).

Over the past two hundred years worldwide urbanization has increased and accelerated greatly during the 20th century (Cohen, 2003). Two hundred years ago,

approximately 1 in 50 people lived in cities, while today more than 1 in 2 people reside in urban areas (Lee, 2009). Cohen (2003) stated that of the projected 2.2 billion people added to the world in the next 20 years, approximately 2.1 billion will be in urban areas. During this time, urban populations will increase at a rate of 1.8% per year, which is twice the projected rate of global population increase during the same period (Cohen, 2003). Serious challenges exist with such rapid and unprecedented population growth in cities with millions of people (Brockerhoff, 2000) and "climate and weather studies encompassing the urban environment will be critical to meeting [these challenges]" (Lee, 2009). Further, the current and projected growth rate in urban areas would require one city of one million residents created every week for the next 40 years just to keep pace with the population growth (Cohen, 2005).

During the next five years, the number of cities with at least one million residents is projected to reach 564, which in contrast, is dramatically larger than 195 cities of this size in 1975 (Brockerhoff, 2000). This increase in large cities is not only due to population growth from new births, but also from (a) the migration of people from rural areas into cities and (b) from the transformation of rural settlements into urban areas (Cohen, 2003).

Not only are urban areas becoming more abundant and populated, they are becoming more densely populated. The world's average population density was 45 people per square kilometer in 2000 and is projected to rise to 66 people per square kilometer in 2050 (and as high as 93 people per square kilometer in some regions; Cohen, 2003). Cohen (2003) also noted that, given that only about 10% of the land is arable on the global scale, the population densities per unit of arable land would be roughly 10 times higher. Brockerhoff (2000) states that the future will be not just an urbanizing world, but a world

in which people are more likely to be residents of very large cities, or megacities of 10 million residents or more. Such cities are already more numerous than ever before.

Urban Meteorological Studies

Over the past 40 years, the study of the meteorological conditions within and their impacts from the urban environment have gained increased interest in atmospheric and climatological disciplines. Oke (1974; 1979b; 1980) pioneered the study of urban meteorology through extensive work along with others (Changon, 1981,1992; Jones and Suckling, 1983, Landsberg, 1981a, 1981b; Unger et al., 2001) who demonstrated how conditions, such as temperature, wind speed, and boundary layer depth, are altered by the presence of large expanses of city structures. Further, their work demonstrated that these impacts could be seen at the mesoscale level.

The most noticeable impact by humans to the atmospheric conditions of the urban environment is the presence of urban heat islands which has been extensively studied across the globe (Arnfield, 2003) including North America (Basara et al., 2008; Schroeder et al., 2010; Ackerman, 1985; Jauregui, 1997; Kim, 1992; Kukla et al., 1986; Magee et al., 1999, Runnals and Oke, 2000, Schmidlin, 1989), South America (Figuerola and Mazzeo, 1998), Europe (Johnson, 1985; Klysik and Fortuniak, 1999; Moreno-Garcia, 1994; Shahgedanova et al., 1997; Unger, 1996; Yagüe et al., 1991), Asia (Kumar et al., 2001; Nasrallah et al., 1990; Park, 1986; Wang and Liu, 1982), Africa (Adebayo, 1987), and Australia (Morris and Simmonds, 2000). These demonstrated that urbanization can lead, with the proper synoptic conditions, to periods where urban core can be in excess of 10.0°C warmer compared to the rural areas of metropolitan areas at a given time.

A better understanding of how surface variability alters the urban environment has been a focus of many recent studies including water balance (Grimmond and Oke, 1986, Grimmond et al., 1986, Mitchell et al., 2008, Wang et al., 2008), evapotranspiration (Grimmond et al., 1991, Taha 1997), aerodynamic properties (Grimmond and Oke, 1999a; Grimmond et al, 1998, Li et al., 2007, Baik et al., 2009), heat storage (Grimmond and Oke, 1999b; Grimmond et al., 1991, Meyn and Oke, 2009), and botanical influences (Grimmond et al., 1996, Alexandri and Jones, 2008). Other studies have investigated how different surfaces resulted in altering the partition of heat fluxes (Anandakumar, 1999) and how they resulted in additional transport of heat into the subsurface (Asaeda et al., 1996). Carlson et al. (1981) used satellite estimations over Los Angeles, California and Saint Louis, Missouri to infer the distribution of surface heat and evaporative fluxes as well as thermal inertia, which all have been theorized to lead to enhanced urban heat island impacts.

Additionally, there has been extensive research on how the structure of cities alters the impacts to the atmospheric conditions. As with many urban meteorological studies, temperature was a main focus of many of the urban geometry impacts including nocturnal temperatures (Arnfield, 1990b; Eliasson 1996a), street-level temperatures (Barring et al., 1995), ground shadowing impacts (Swaid and Hoffman, 1990-91), and urban heat islands (Oke, 1981; Eliasson, 1994; Barring et al., 1995; Eliasson, 1996b). Further studies focused on other aspects of impacts from city geometry such as wind flow (Cionco and Ellefsen, 1998), dispersion (Johnson and Hunter, 1995), and surface radiation budgets (Frank et al., 1981b; Voogt and Grimmond, 2000; Champan et al, 2001).

The boundary layer is an important aspect of understanding the near surface processes occurring above metropolitan areas. The work by Hildebrand and Ackerman (1984) demonstrated that the presence of an urban environment dramatically impacts urban heat fluxes (by two to four times that of the rural fluxes), creates larger magnitudes of moisture fluxes at upper levels, and results in greater urban turbulences intensities aloft. While most studies analyze large metropolitan area impacts on the boundary layer, Tapper (1990) showed that these impacts can be measured even over much smaller urban areas thus showing the noticeable impacts from just minor land-use changes.

Urban Atmospheric Modeling

Through the use of various computer models, theoretical hypotheses focused on the impacts of the urban environment on various atmospheric conditions can be tested. Similar to the observational studies that will be outlined in Chapter 5, most of the urban atmospheric modeling studies focused on urban temperature / urban heat islands or the energy balance and partition of fluxes related to the presence of an urban environment. While the presence of urban heat islands had been well documented scientifically, other studies have sought to determine if non-measured variables critical to the determination of the urban heat island could be simulated. Hafner and Kidder (1999) demonstrated that, through the use of Advanced Very High Resolution Radiometer (AVHRR) satellite data, surface parameters such as soil temperature and moisture could be modeled to impact the presence and intensity of urban heat islands. Herbert et al. (1998) used numerical models to determine the thermal climate within a city canyon, while Richiardone and Brusaca

(1989) were able to use a model to alter stability and surface heat fluxes to show their impacts on different urban heat island intensities.

The modeling of urban environment impacts on the surface energy balance has also been extensively analyzed. Sakakibara (1996) utilized models to compare a parking lot with an urban canyon to show that the urban geometry contributed greatly to the alteration of the surface energy budget and thus the formation of urban heat islands. Sivers and Zdunkowski (1985) showed from an extension of the work by Aida and Gotoh (1982) that not only does the presence of urban canyons impact the albedo within the city, but the orientation of the buildings and more so the orientation of the streets impacts the variations of the albedo. Taha (1997) demonstrated that, by modifying an existing mesoscale model with an objective hysteresis model, the impacts of surface modification and their resulting surface fluxes are more pronounced than in an unmodified mesoscale model. Grimmond et al. (2010) compared 33 numerical models on their performance in simulating fluxes in the urban energy balance and to determine the level of model complexity needed to accurate simulate the fluxes. Similarly, Grimmond et al. (2011) compared 32 urban land surface schemes through a four-stage systematic evaluation. In both studies, the results showed that no particular model or scheme performed better that the rest across all of the flux simulations; however, the selection of parameter values can have large impacts on the resulting simulations.

Oklahoma City

Oklahoma City, Oklahoma, USA, is located in the south-central part of the United States and represents a typical, rapidly growing urban area in North America. Founded in 1889, its aerial extend covers nearly 1610 km^2, which makes it one of the largest cities

by land area in the United States. Despite its large spatial extent, only approximately 630 km^2 is defined as an urban area. However, over the past century, its urban area continues to rapidly expand outward and is projected to continue to expand in the future.

The United States Census Bureau's latest estimation lists the Oklahoma City metropolitan area (i.e. the geographic area that consists of Oklahoma City and its surrounding suburban areas) at a population of just over 1.2 million residents. This is a 10.1% increase in population from the 2000 census and ranks it as the 44th most populated metropolitan area and 31st most populated urban area in the United States (United States Census Bureau, 2009; United States Census Bureau, 2009). Figure 3 shows the urban and rural population trends from 1950 to 2050 of the United States and Oklahoma City. This data demonstrates that, over the past 60 years, Oklahoma City has a higher rate of urban population increase than the United States mean and is projected to grow at the same rate over the next 20 years.

Oklahoma City is an ideal choice for urban modeling study for many reasons. It resides in relatively flat terrain (Fig. 4) with elevations of approximately 330 m above mean sea level just to the east of the city to 420 m just west of the city leading to an elevation change of less than 100 m across a distance of 100 km. River valleys run from west to east through the city, but are very shallow. Additionally, there are no large bodies of water adjacent to the urban core. As a result, these optimal features limit complicating errors and factors which can be associated with surrounding geography. Further, the region is heavily monitored by in situ and remote sensing instruments focused on observing atmospheric conditions. The nested atmospheric observing networks yield

excellent input and verification data for any numerical simulations of the urban and adjacent rural environments.

Chapter 3: Observational Data

Oklahoma Mesonet

The Oklahoma Mesonet (Fig. 5) is an automated network of 121 remote, meteorological stations across Oklahoma (Brock et al., 1995; Shafer et al., 2000; McPherson et al., 2007). Each station measures core parameters that include: air temperature and relative humidity at 1.5 m, wind speed and direction at 10 m, atmospheric pressure, downwelling solar radiation, rainfall, and bare and vegetated soil temperatures at 10 cm below ground level. In addition, over 100 sites measure air temperature at 9 m. In an effort to avoid anthropogenic influences, most Oklahoma Mesonet sites are located in rural areas. Mesonet data are collected and transmitted to a central point every 5 minutes where they are quality controlled, distributed and archived (Shafer et al., 2000; McPherson et al., 2007).

Oklahoma City Micronet

The Oklahoma City Micronet (OKCNET) was an operational network designed to improve atmospheric monitoring across the Oklahoma City metropolitan area (Basara et al, 2011). The 40-station network consisted of four Oklahoma Mesonet Stations (OKCE, OKCN, OKCW, and SPEN) and 36 stations mounted on traffic signals at a height of approximately 9 m and station spacing of approximately 3 km. At each traffic signal site, atmospheric conditions of air temperature, humidity, pressure, rainfall, wind speed, and wind direction were measured and transmitted every minute to a central facility 24 hours per day, year-round where they were quality controlled, distributed, and archived using the Oklahoma Mesonet infrastructure. The Oklahoma City Micronet included a cluster of stations within the central business district as well as stations throughout the Metropolitan

area (Fig. 6). Basara et al. (2008) showed that air temperature measurements in the urban areas show little difference between 2 m and 9 m during the night time when urban heat islands are most prevalent (Fig. 7), which indicates that comparisons of air temperatures can be made between Oklahoma City Micronet (9 m) and the Oklahoma Mesonet (1.5 m).

Urban Heat Islands

Temperature and apparent temperature values measured in densely urbanized areas have been shown (and felt) to be warmer temperatures than surrounding rural areas (Basara et al., 2010). The warmer temperatures typically peak in magnitude shortly before sunrise and are the result of the difference in thermal storage of urban areas (e.g. concrete, asphalt) and rural areas (e.g. grasslands). These warmer temperatures are referred to as urban heat islands due to their spatial uniformity (and "island" shape) with relation to the urban area. An urban heat island index (UHII) is a measure of the strength of an urban heat island and is the difference between the urban temperature and the rural temperature (Eq. 1; Ackerman, 1985; Oke, 1987).

$$UHII = (T_{Urban} - T_{Rural}) \quad (1)$$

The definition or calculation of urban and rural temperatures varies across studies but typically involves the averaging of several independent observations of those influenced by urban land use (e.g. "urban") and those sufficiently removed from any urban influence (e.g. "rural). The UHII is difficult to accurately calculate when representative urban

measurements are not available, which occurs in many metropolitan locations where meteorological measurements are observed in the outer parts of cities (e.g., airports). If multiple measurements of urban and rural measurements are available (as with the Oklahoma City Micronet and the Oklahoma Mesonet), then the UHII can be determined by taking the difference of the mean urban and mean rural temperatures (Kim and Baik, 2005; Basara et al., 2008) and can provide a more accurate measurement of the UHII by reducing the variability between temperature observing sites (Hawkins et al., 2004; Basara et al., 2008). An example of an urban heat island measured by the Oklahoma City Micronet is shown in Figure 8. Arnfield (2003) stated that UHII is "the most well documented example of anthropogenic climate modification". However, through the results of this research, it will be demonstrated that this statement, while true, is a bit incomplete as there are more factors beyond anthropogenic sources that contribute to the UHII.

The research presented in the following chapters utilizes a variety of new approaches to calculating the UHII. The standard UHII equation as shown in Eq. 1 will be utilized in two different methods: (1) through measurements taken at specific site locations where observations stations were located (e.g., Oklahoma Mesonet stations at Chandler, El Reno, Guthrie, Kingfisher, Minco, Norman, Oklahoma City East, Oklahoma City North, Oklahoma City West, Shawnee, and Spencer), and (2) through arbitrary locations specifically chosen for their strong urban and rural representativeness. Additionally, the UHII is analyzed through non-stationary methods where maximum urban values from varying quantities of numerical model grid points ensure that the warmest locations are utilized regardless of their exact location. By implementing several new and original

approaches to the UHII calculation, a more complete understanding of the urban heat characteristics is accomplished and limitations of each UHII approach can be minimized through the strengths of other UHII approaches.

Chapter 4: Numerical Urban Modelling System

Candidate Days

To ensure that the WRF model can resolve urban heat island signatures from Oklahoma City, five data cases were analyzed across varying seasons. By using days throughout the calendar year, a determination can be made as to the impact of seasonal varying background fields (e.g. relative greenness, downwelling solar radiation) or input data fields (e.g. air temperature, humidity) may have on the model's ability to accurately resolve the urban meteorological signatures. Candidate days (Table 1) were chosen that included weak synoptic conditions (e.g. light winds, clear skies, and no rain) for a 24-hour window before and after the modeled period. Additionally, days were chosen that had distinct urban heat islands measured by the Oklahoma City Micronet and the Oklahoma Mesonet to allow for model verification.

The Weather Research and Forecasting (WRF) Model

The Weather Research and Forecasting (WRF) model (http://www.mmm.ucar.edu/wrf/users/docs/arw_v3.pdf) was developed through a partnership between the National Center for Atmospheric Research (NCAR), the National Oceanic and Atmospheric Administration (NOAA), the National Centers for Environmental Prediction (NCEP), the Forecast Systems Laboratory (FSL), the Air Force Weather Agency (AFWA), the Naval Research Laboratory, the University of Oklahoma (OU), and the Federal Aviation Administration (FAA). The WRF model being used for this study is version 3.5 and compiled as the Advanced Research WRF (ARW, previously called EM) with the nesting options enabled. Table 2 shows the WRF and WRF Preprocessing System (WPS) options

utilized in the model runs including the radiation schemes, boundary layer schemes, and urban canopy model activation. Anthropogenic heating was turned off for the model runs due to anthropogenic heating constants being set to modern values which were not representative of past, historical conditions. For example, due to the nature of this study, anthropogenic heating for historical runs would introduce a warm bias from stronger heat sources (e.g. air conditioners, automobiles, etc.) that did not exist in the early part of the 1900's. The computing for this project was performed at the OU Supercomputing Center for Education & Research (OSCER) at the University of Oklahoma (OU).

Domains

The WRF model was run in a five domain configuration with 2-way nesting to allow the inner domains to feedback to the outer domains and vice versa. All domains were centered over Oklahoma City and have the following characteristics:

- Domain 1 : 4050km x 4050 km with 40.5km grid spacing
- Domain 2 : 1350km x 1350 km with 13.5km grid spacing
- Domain 3 : 450km x 450 km with 4.5km grid spacing
- Domain 4 : 150km x 150 km with 1.5km grid spacing
- Domain 5 : 50km x 50km with 500m grid spacing

Figure 9 displays the domains with the Oklahoma county boundaries and neighboring state outlines indicated. Domain 5 is the domain focused upon in this study.

Input Data / Background Fields

Input meteorological data and background fields in the WRF model used for this study were assembled from various sources. The 32 km National Centers for Environmental Prediction (NCEP) North American Regional Reanalysis (NARR; Mesinger et al., 2006) data files were used for the surface and upper air data initialized into the WRF model runs. The NARR files exist on the Eta 221 grid at 29 pressure levels created every 3 hours and are generated from the Eta 32 km / 45 level model and include many meteorological variables including temperature, wind, moisture, pressure, and surface fluxes. The NARR files created by NCEP utilized radiosonde data, such as air temperature, wind, and moisture, as well as meteorological data from surface observing stations, satellites, and aircrafts.

The land use dataset is the United States Geological Survey (USGS) National Land Cover Database (NLCD; http://www.mrlc.gov/). This study used the 2011 NLCD which has 24-categories of land data types at 30 arc second (~1 km) spacing and the dataset included four urban categories (open space, low, medium, and high intensity).

As the main part of this study focuses on how the land surface conditions had changed in the Oklahoma City region since its inception in 1890, a historical analysis of the area was analyzed. Historical land use ingested into the WRF model were created from a variety of sources including the City of Oklahoma City, U.S. Department of Commerce Bureau of the Census, U.S. Department of Agriculture, and the Oklahoma Water Resources Board.

The City of Oklahoma City provided historical analyses of water and sewage pipelines for every decade back to 1900. These maps indicated where urban areas existed

as well as the infrastructure for urban development. The U.S. Department of Commerce Bureau of the Census data was utilized to help determine the size and extent of population areas in the areas surrounding Oklahoma City (e.g. Edmond, Moore, Norman, etc.). The U.S. Department of Agriculture maintains historical records of agriculture yield production, which was used to determine the extent and spread of "cultivated crops" (Category 82 in the NLCD) in each county. The Oklahoma Water Resources Board archives historical records of every lake in Oklahoma including when each lake was built/dammed. Additionally, general historical records of the creation of major large urban features, such as Will Rogers World Airport, Tinker Air Force Base, and interstate highways, were utilized in the development of the historical mapping of the land use of the greater Oklahoma City area. Figures 10-14 show the historical information with which each of the tridecadal periods' background land use maps were created.

As a result of the assimilation of historical land use features, land use maps for 1890, 1920, 1950, and 1980 were created; the land use map for 2011 was already created from the NLCD imagery. In 1890 (Fig. 10), urban areas did not exist, lakes were not present (just the free-flowing rivers), and the vegetation was native consisting of grasslands as well as evergreen and mixed forests with no cultivate crops. By 1920 (Fig. 11), small urban areas had begun to develop and farming became very widespread. In 1950 (Figure 12), the urban areas began to expand outward, an urban core to Oklahoma City began to develop, and lakes began to be formed to provide water to the growing city. By 1980 (Fig. 13), urban explosion and rapid growth had occurred and surrounding cities (suburban areas) also began to rapidly develop. Finally, in 2011 (Fig. 14), expansion of the

metropolitan area continued and existing urban areas developed higher population densities.

The Uncoupled High Resolution Land Data Assimilation System: HR-LDAS

The uncoupled High Resolution Land Data Assimilation System (HR-LDAS; Chen et al., 2007) was developed by the National Center for Atmospheric Research (NCAR) to initialize land surface input files before utilizing them in the coupled WRF model. It utilizes the Noah land surface model (LSM) initially developed by scientists at Oregon State University (Pan and Mahrt, 1987) and updated by scientists at the National Center for Environmental Prediction (NCEP) and the National Center for Atmospheric Research (NCAR). The HRLDAS uses the same parent and nested grids as those for the WRF model runs and combines land use, soil texture, soil moisture, vegetation, terrain, and other land surface parameters (Chen et al. 2007) to generate its background output which is used as updated input for the WRF model. Nemunaitis (2014) showed the improvements of utilizing a multi-year spin up of runs with five years of spin up prior to any WRF model runs. Figure 15 shows the WRF initialization field of soil moisture conditions at a 1 km grid spacing using just NARR initial conditions and no NLDAS spin-up and using a 5-year spin up of NLDAS and NARR initial conditions (Nemunaitis, 2014). All model runs utilized in this study included five years of HR-LDAS spin-up utilizing NARR data applied to the initial conditions.

Chapter 5: Run-time Accuracy

An optimal model run time must be selected for any model simulations to ensure the most representative model output to actual conditions. Model run times that are too short may not allow the model physics to completely spin-up, while model run times that are too long begin to compound slight individual time step errors into large output errors. Past urban heat island modeling studies have used a variety of model run time from 24 hours (Miao et al., 2008), to 36 hours (Lin et al., 2008), to 60 hours with discarding the first 6 hours (Salamanca et al., 2012) or 12 hours (Giannaros et al., 2013) of output. However, none of the studies justified the selection of their model run time lengths. Unlike other past numerical model studies, this study performed a sensitivity analysis of different model run times across a variety of case studies to determine the optimal run-time needed to observe urban heat island signatures from the WRF model with minimal difference between observed values before selecting a run time for the model simulations.

For each candidate day, the model was initialized at 18 hours before (e.g. 18-hour run-time) the desired output time (1200 UTC) and run with a given set of initial atmospheric and land-use conditions. The output time of 1200 UTC was chosen to correlate closely to the time of peak urban heat island intensities. The run-time length was then increased by six hour intervals out to 48 hours and the process was repeated. The UHII were calculated from model grid points located where Oklahoma Mesonet and Oklahoma City Micronet stations existed. After all run-time lengths were completed, a statistical analysis comparing UHII from model output to actual observations was performed on each model run-time to determine the optimal run-time for the WRF model given the parameters of the overall study.

21 June 2008 Case Study

The results of the analysis from this case study are shown in Figure 16a (urban) and Figure 16b (rural). The verification of average air temperature data is via the dashed line with the maximum and minimum values indicated by the shaded envelope. The main focus on this case study is in the 01 to 03 UTC timeframe, which was selected due to the least difference of the model output's values compared to the observations across all-time series runs. Mean error values of the model runs from the observational data are shown in Table 3.

For the urban results (Fig. 16a), the individual runs behave differently from each other. The 48 and 42-hour runs were colder by ~1°C in the late afternoon (18 - 23 UTC) and the 48-hour run was warmer during the middle of the night (04 - 09 UTC). The shorter runs (18 - 36 hour) were warmer by ~2°C in the late afternoon and colder near sunrise. Overall, all of the model runs urban values performed very well in the 01 - 03 UTC timeframe with mean error values less than 0.67°C and the 24 and 30-hour performing exceptionally well with mean error values less than 0.40°C.

For the rural results (Fig. 16b), the run results were similar in pattern to the urban results. The 48 and 42-hour runs were colder in the late afternoon (18 - 23 UTC) by ~2-3°C and warmer during the middle of the night (04 - 09 UTC) by ~2°C. The shorter runs (18 - 36 hour) were also warmer in the late afternoon and throughout the night by between 1°C and 2°C and very close to verification near sunrise with errors of 1.0°C or less. Overall, all of the rural values from the model runs performed slightly worse than the urban values but had mean errors less than 2°C in the 01-03 UTC timeframe and the 24 and 30-hour performing exceptionally well with mean error values just above 1.0°C.

From an urban heat island index standpoint, the results from this case study looked very well. Figure 16c shows the run time accuracy of the urban heat island index for each of the model run time lengths. During the afternoon hours, the model runs were approximately 1°C above the verification value of near 0°C but well within the maximum and minimum envelope of between 1.5°C and -2.5°C. All of the model runs showed an increase in the urban heat island index at 00 UTC and increased over the next few hours to plateau at 02 UTC to a value of ~2.5°C in a similar pattern to the verification data which had a plateau of ~3°C. However, the model runs all had lower urban heat island indices than the verification throughout the night by less than 1°C, but the 24-hour run had the values to the verification data with errors between 0°C and 1°C.

Additionally, an analysis was performed on the historical perspective of the 24-hour model simulations with each of the tridecadal land use backgrounds. This unique analysis will track how the nocturnal time series of UHII changes from urban development. The comparisons of historical 24-hr UHII simulations for 21 June 2008 case study (Fig 16d) demonstrated that as the urban area grew over time, the UHII values from the model simulations transitioned closer to verification with each successive period. The 1890 model simulation had static UHII values near 0°C with UHII values from successive runs increasing by approximately 0.5°C in the 01-03 UTC timeframe.

1 August 2008 Case Study

This late summer case had one run time perform much better than all of the other run times in the study. The run time accuracies for this case are shown in Figure 17a and the mean error statistics in Table 4. All of the run times have very similar patterns, which

also match the pattern of the verification data. While the 48-hour run time showed the coldest urban results, it matched best to the verification data being within 0.5°C throughout most of the simulation period. Similarly, the rural run time accuracy (Fig. 17b) behaved similarly to the urban accuracies in that all runs matched the verification profile pattern and that the 48-hour run was the coldest and closest to the verification data. Again, the 48-hour run was within 0.5°C throughout most of the period.

However, from an urban heat island index perspective (Fig. 17c), the 48-hour run time wasn't always the closest to the verification data. This result shows that while the other model run times may not have had as accurate urban and rural values, their differences (e.g. urban heat island indices) were more accurate. Thus, one must consider all aspects of the analysis when considering the true value and accuracy of a model run. Depending upon the verification time, most all of the model run times were similar to one another with errors of approximately 1°C with a slight edge to the 42-hour run time which was less than 0.5°C for much of the time period, especially during the 05-07 UTC time frame.

Analyzing the 24-hour run times over time (Fig. 17d), the 2011 land use information had the closest results to the verification data, as expected, with errors between 0°C and 1.5°C throughout the night. However, the earlier years were not stratified uniformly by historical age. This is likely due to varying differences from verification of either the urban or rural components leading to differing errors in the urban heat island indices.

5 September 2008 Case Study

The model run time accuracies from this case had very strong results to the urban (Fig. 18a) and rural (Fig. 18b) verification data and the mean error statistics (Table 5)

also show low difference from the observations. For the urban results, most of the model run times remained within the very narrow 2°C verification envelope through the late afternoon and early evening indicating very accurate and consistent simulations of the urban environment. At approximately 05 UTC, the model results began to diverge from each other and transitioned from an error of less than 0.5°C to over 4.0°C. However, the 18 and 24-hour model runs remained very close to the verification data with errors of less than 1.0°C. For the rural results, the model runs again remained consistent with each other and verification during the afternoon hours being within 1.0°C, but began to diverge near sunset (e.g., 01 UTC) whereby differences were as much as 3.0°C. The 42 and 48-hour model runs had the closest results to verification (within 1.0°C) throughout the evening and the 36-hour run time became most accurate just before sunrise (e.g., 10 UTC). The pattern and slopes of all of the model run times matched the verification very well, which indicates that the model runs grasped the nocturnal cooling rates accurately in the rural areas, but the initial air temperature values at sunset led to difference overnight.

The model runs' accuracy of the urban heat island indices (Fig. 18c) showed less accurate results than the individual urban and rural component simulations. During the late afternoon, most of the models had higher urban heat island indices by approximately 0.5°C than the verification data. Near sunset (e.g., 00 UTC), all model runs increased the urban heat island index to between 2.0°C and just under 3.0°C, but not as high as the verification data which reached near 4.0°C. This particular case had a different than normal verification data pattern of urban heat island indices in that instead of remaining high or slightly increasing throughout the night time hours, these values dropped by ~2.0°C at approximately 03 UTC before slowly increasing 1.0°C over the next few hours.

Most of the model runs behaved similarly to the initial decrease in urban heat island index, but did not slowly increase as the verification data and instead slowly decreased approximately 1.5°C throughout the night. The 24-hour model run remain much warmer than the other model runs during the night staying within the verification envelope until just before sunrise.

An analysis of the 24-hour run time simulation comparisons for this case (Fig. 18d), shows that the 2011 land use values did show the closest urban heat island index values to the verification data with errors close to 0°C in the afternoon and between 0°C and 2°C throughout the evening. However, the 1950 land use values best matched the overall unique time series pattern of this case, but its peak urban heat island index was a few hours behind the verification data.

15 September 2008 Case Study

The urban run time accuracies of this case (Fig. 19a; Table 6) were warmer for all of the model run times in the late afternoon and early evening by between 1.0°C and 3.0°C. Due to a stronger cooling rate in the model run times, between 05 and 09 UTC all of the model runs transitioned to having cooler urban air temperatures than verification by between 0.5°C and 2.0°C by sunrise. The 24-hour model run time had the weakest cooling rate, and thus, was the most accurate of all of the model run times in predicting the urban air temperatures over the entire time period.

The rural run time accuracies (Fig. 19b; Table 6) once again showed between 1.0°C and 3.0°C warmer air temperature values than the verification data for all of the model runs. However, the rural cooling rate in the models matched the verification cooling rate

and thus the modeled rural air temperature values remained warmer than the verification data during the entire time period. Overall, the 24-hour model run time had the closest rural air temperature values to the verification data throughout the time period with errors of between 1°C and 2°C.

From an urban heat island index viewpoint, all of the models had much smaller temporal changes than the verification data as seen in Figure 19c and Table 6. The model runs had higher UHII values by nearly 0.5°C during the late afternoon, increased as expected during early evening, but remained much lower by approximately 2.0°C throughout the night. While the UHII values produced by model runs remained in the envelope for more of the time period, the envelope was much larger than in other cases ranging from 1.0°C to near 7.0°C. Analysis of the 24-hour historical simulation comparisons (Fig. 19d) shows that the 2011 land use values only performed slightly better than the 1950 land use values with both having values approximately 2°C lower than the verification data.

15 March 2009 Case Study

This case was much different than the others given that it was a cold weather case. The run time accuracies of the urban air temperatures (Fig. 20a; Table 7) were within 0.5°C during the late afternoon and early evening except the 24-hour run which was approximately 2°C to 3°C cooler than verification during this period. However, at 01 UTC, all of the model runs had very strong cooling rates in the urban environment, but the verification data had a much lower cooling rate. These strong cooling rates only seen in this case study may be the result of the different urban parameters utilized by the WRF

model in wintertime simulations. As a result, by sunrise there were differences from 4.0°C to as high as 5.0°C in urban temperatures between each of the model runs and the verification data.

The rural temperature analysis of the run time accuracies (Fig. 20b; Table 7) was much different than that of the urban air temperature analysis for this case. Throughout the entire time period, all of the model runs very accurately matched the verification data and were within 1.0°C for almost the entire period. The model runs had nearly the same cooling rate of the rural air temperatures as with the urban air temperatures, but this cooling rate matched that of the verification data.

The run time accuracies of the UHII values (Fig. 20c; Table 7) were fairly close in the afternoon hours being within 0.5°C with the exception of the 24-hour run which was about 1.0°C cooler. However, they did not respond well during the night time hours after its initial increase around sunset. As the verification values of urban heat island indices remained between 3.0°C and 4.0°C, the model runs values decreased to below -1.0°C during the night. This large difference is likely the result of similar cooling rates in the urban and rural temperatures when the two cooling rates were much different in reality. Overall, all of the model run times performed poorly during the peak of the UHII with errors greater than 4°C. Comparing the 24-hour simulation comparisons historically (Fig. 20d) showed little variation due to land use changes and all were 2°C to 5°C cooler than the verification. For this winter case, the WRF model actually simulated an urban cool island rather than the actual urban heat island. As such, the WRF model had difficulties accurately simulating the urban heat island for this cold weather case.

Summary

With the exception of the colder weather case, the WRF model simulated the urban heat island development from late afternoon to early morning in Oklahoma City. In some cases, the magnitudes of the rural and urban temperature components varied by 1.0°C or more, but the resulting UHII values remained within 0.5°C to verification data. Overall, the 24-hour run time provided the most accurate results across the variety of scenarios in which the WRF model was run. From the five case studies (Tables 3-7), the 24-hour run time simulations resulted in the lowest mean error in three of the cases and was within 1.0°C for the other two cases. As a result, the remainder of the research presented will utilize 24-hour run times of the WRF model.

Chapter 6: Urban Heat Island Changes Over Time

After determining the most accurate WRF model run-time from the Run-time Analysis (see Chapter 5), a historical analysis of urban heat island evolution was performed. While there has been much documentation of a variety of urban heat modeling studies, this study is unique in its analysis of urban heat islands from a historical perspective. The addition of the fourth dimension of time to an urban heat study provides a view of the temporal development of urban heat islands that no other study has shown. For each tridecadal simulation, all input data remained the same with the exception of the land use background field which was altered (see Chapter 4) to represent the spatial dimensions of the Oklahoma City urban areas at each tridecadal period. For this study, climatic trends were not accounted for as the goal was to determine how the specific urban areas were impacting the surrounding meteorological conditions. For each case study, the particular hour of focus was determined from the simulation output hour in which the maximum indication of urban heat island values from the simulation occurred. Additional analysis was performed to better demonstrate the urban growth impacts by calculating the difference between a model simulation (e.g., 1920, 1950, 1980, or 2011 land use model simulations) and the initial state (e.g., 1890 land use model simulation). The initial state model simulation indicates the natural variability of the air temperature values which has no influence from any urban development and is an aspect of this research that has not been utilized by any other urban heat development studies. This natural variability is the result of differences in elevation (e.g. river valleys) and land use (e.g. forest, grasslands, prairie, etc.).

21 June 2008 Case Study

The 2-m air temperature values at 02 UTC from the 24-hour model simulations of 21 June 2008 are shown in Figure 21 for the five tridecadal periods. In 1890, the urban core area cannot be detected; however, terrain influences can be seen. The higher terrain to the west is indicated by slightly warmer temperatures of nearly 3°C compared to the various river valleys (including the Oklahoma River which runs through Oklahoma City), which can be seen by the locally lower temperatures. Given that the land use for 1890 was consistent with no urban land use values, this output indicates that the natural variability of air temperatures without any influences from the metropolitan area are on the order of 1-2°C within the study domain. In 1920, the city grew with slight warming of approximately 1°C in the Oklahoma City core. For the 1950 simulation, the urban air temperatures were about 3°C warmer than the surrounding areas and more pronounced not only in Oklahoma City but also in Norman to the south. Due to the urban development explosion in 1980, the strong urban air temperatures, approximately 4-5°C warmer than rural areas, are clearly shown. Finally, by 2011, the warm air temperatures remained approximately 4-5°C warmer than rural areas but expanded further into the surrounding areas. Additionally, cooler temperatures over lakes within the Oklahoma City area created localized minimum air temperatures.

By subtracting out the natural variability seen in the 1890 results, the true impacts of urban growth over time can be more clearly analyzed. These results are shown in Figure 22, which is the air temperature difference between the 1890 land use model run and each of the other tridecadal model runs. In 1920, the growth over the small urban core is indicated by the 1°C to 2°C bullseye of air temperature difference. In 1950, the urban

expansion and development of surrounding cities is seen as well as 3°C to 5°C warmer temperatures in the urban core. From 1980 and 2011, the dramatic increase in both spatial coverage and intensity can be seen with temperature differences reaching over 5°C across large portions of the metropolitan area.

Another unique benefit of utilizing temperature difference maps is the elimination on non-uniform, rural air temperature fields. Each of the maps in Figure 21 show that the rural areas vary from 1-5°C depending upon whether the observation is in the cooler, lower terrain of the east versus the warmer, slightly higher terrain of the west. Thus, the urban heat island calculation might vary depending upon which rural location(s) are considered. The difference maps allow for the true difference in air temperature values from urban to rural as a result solely on urban development to be calculated.

1 August 2008 Case Study

Figure 23 shows the 2-m air temperatures at 06 UTC for the 1 August 2008 case study for each of the tridecadal periods. This case study had the hottest air temperatures of all of the case studies and was one of the hottest days of 2008 with temperature values over 32°C. Similar to the 21 June 2008 case, there are only slight changes of 1°C to 3°C from 1890 to 1920 to 1950 as the Oklahoma City urban area began to grow. The urban air temperatures then rapidly expanded with the urban expansion in 1980 and continued through to 2011 with urban air temperatures increasing by over 5°C. Once again, the warmer areas to the west from the higher terrain can also be clearly seen.

By removing the natural variability from the 1890 land use model run, the increase in the 2-m air temperature values over the urban areas are more clearly seen (Fig. 24). Again,

slight 1°C to 3°C urban air temperature increases can be seen for 1920 and 1950 before the significant urban growth by 1980 shows dramatic increase of over 5°C in the urban air temperature differences. The impact of both Lake Hefner and Lake Overholser are also clearly indicated in the northwest and west, respectively, parts of the Oklahoma City area.

5 September 2008 Case Study

Due to a slight south-westerly wind in this case, the 2-m air temperature results at 02 UTC for this case (Fig. 25) show downwind impacts from heat advection at source points of higher elevation to the west. Similar air temperature magnitude increases remain for each of the five time periods as compared to the previous two cases; however, the surrounding urban areas (e.g. Norman to the south, Edmond to the north) are more pronounced. The air temperature differences (Fig. 26) are once again similar to the previous cases with the slight indication of the influences from the wind. The 2-m air temperature values increased by over 5°C in the Oklahoma City urban area over the 120-year time frame.

15 September 2008 Case Study

The 2-m air temperature results at 02 UTC for this case (Fig. 27) are again impacted by advection of the air temperatures downwind from the source regions. In this case, the winds are slightly from the north, which can be seen as warmer areas are advected slightly to the south, especially in southern Oklahoma City and Norman. The river valley temperatures from the model simulations are more noticeable in this case showing the

natural variability. These larger river valley temperatures of about 2°C led to smaller increases in air temperature differences (Fig. 28) of 1°C or less through the middle of the Oklahoma City urban core (where the river runs). Since the arbitrarily selected urban location lie within the river valley, the statistical comparisons of urban core changes utilizing traditional UHII calculations over time may be limited in explaining the entire urban impacts. Future explanation of alternate methods for statistically analyzing urban growth are presented in Chapter 7.

15 March 2009 Case Study

This final case study had the coldest air temperatures (~10°C) and shows the least significant results over time. The 2-m air temperature values at 03 UTC are shown in Figure 29. The values from 1890 to 1920 to 1950 show almost no noticeable change over time with air temperature changes at or below 1.0°C over the first 60 years. During the urban expansion periods of 1980 and 2011, there are slight increases of approximately 2.0°C in the air temperature around Oklahoma City; however, the urban core of the city remained cooler by approximately 1°C to 2°C or slightly decreased. The air temperature difference maps (Fig. 30) better demonstrate these changes over time. The WRF model had difficulty in its resolution of the urban land use categories during colder weather. However, additional statistical methods utilizing the WRF output from this case study do show urban impact results and are shown in Chapter 7.

Summary

Overall, the spatial extent and magnitude of near surface air temperature increases of a developing urban area over time was shown through the use of the WRF model runs. The increases in 2 m air temperatures from the development of the metropolitan area were over 5°C in the summer when urban heat is of most concern. The 1890 model runs indicated that even with the removal of all urban land use locations, there still existed a natural background variability to air temperature values of between 1°C and 2°C. This study is unique in that it demonstrated that when analyzing urban heat island indices, one must consider that the value is not just due to urban impacts but also to the natural variability of the areas. In the case of Oklahoma City, its urban area lies in the Oklahoma River valley, which naturally has slightly warmer temperatures of about 1°C to 2°C than its surrounding area. The WRF model did not handle the cold weather case very well from a spatial extent or magnitude point of analysis, possibly due to the different parameters utilized by the model for wintertime simulations. Since this study generated background variability maps, the utilization of difference maps helped better portray the impacts due to just the urban land use growth over time which other urban heat studies could not produce.

Chapter 7: Alternate Urban Heat Island Methodologies

In addition to typical urban heat island characteristics such as urban temperatures, rural temperatures, and urban heat island indices, other metrics can be utilized to portray the spatial extents and magnitude of urban induced air temperatures. This study developed new methodologies for providing unique numerical and graphical representations of the urban heat characteristics beyond just the UHII as previously defined. Through the use of these expanded urban heat representations, this study provides a historical view of urban heat development that has not been shown by other researchers. As part of this study, analyses were performed not only at set locations (either arbitrary or predefined), but at all of the grid spaces in the WRF model output. By doing so, the entire model output analysis was considered rather than just a set number of points. The use of the numerical values from all of the model output grid spaces provides more robust characterizations to be developed through the dramatically increased number of data points available for analysis and allows for numerical urban heat calculations to be generated from a quantity of data points of a few orders of magnitude greater than previous studies.

Verification Siting Issue (Mesonet vs. Selected Rural)

Choosing particular locations in which to calculate urban and rural temperatures must be carefully considered. Typical observation based urban heat island studies utilize existing meteorological stations which can unintentionally introduce biases. The surface observational data in this study is the Oklahoma Mesonet and the Oklahoma City Micronet. While the Oklahoma Mesonet provides valuable rural temperatures measurements and the Oklahoma City Micronet station can provide valuable observations

that represent the urban temperature environment, those precise locations are not necessarily the best location to be utilized in a modeling study. Some of the Oklahoma Mesonet stations considered rural locations in this study (e.g. Norman, El Reno, Chickasha, and Shawnee) are properly sited using World Meteorological Organization (WMO; WMO, 1983) site standards; however, they are fairly close to locations in which urban land use categories exist in a modeling framework. As a result, due to the calculations and averaging that occurs within the WRF system, the grid spaces containing the Oklahoma Mesonet sites have urban induced impacts. To remove these impacts, arbitrary rural locations were selected that were sufficiently removed from grid space locations that contained urban land use categories and urban locations were selected that were within and surrounded by grid spaces containing urban land use categories. The urban locations are shown by five black dots in the urban core of Oklahoma City and the rural locations are shown by eight black dots (one at each cardinal direction) on the model output maps (such as Fig. 21) in this study.

Top 10/100/500/1000 Warmest Locations UHII

Because the WRF model output in this study provides 28,056 points of air temperature data from the output grid, utilizing this large dataset in determining urban heat island characteristics can be accomplished. For the 21 June 2008 case study, a graph of urban and rural temperatures for each tridecadal period utilizing air temperature averages of the previously mentioned arbitrary points for urban and rural values as well as the top 10, 100, 500, and 1000 warmest pixels are shown in Figure 31a. For 1890, the arbitrary locations (e.g., “Urban”) value is lower by about 1°C to 2°C than all of the

aggregated categorical values (e.g., “Top 10”, “Top 100”, etc.). This is due to the fact that the arbitrary location is fixed over the future location of the urban core, while the categorical values take into account warmer higher elevation locations. However, once the city begins to grow, this discrepancy disappears. In this case study, all of the urban air temperature values derived from the warmest temperatures approach (e.g., “Top 10”, “Top 100”, etc.) increase approximately 2°C over time; however, the arbitrary urban air temperature value (e.g., “Urban”) slightly decreases less than 0.5°C from 1980 to 2011 after increasing over 3°C from 1890 to 1980. This slight decrease in the arbitrary air temperature value from 1980 to 2011 may be the result of the values not being the actual warmest locations in the urban area, which demonstrates a key limitation to the typical UHII methodology of static locations for urban and rural location utilized by past research. By utilizing the warmest values approach, it ensures that the maximum magnitude of urban heat values is used when calculating UHII, which may not occur when using the more traditional specific location based approach for urban air temperature values.

Examination of the resulting urban heat island values calculated from the difference between the averaged arbitrary rural locations and either averaged arbitrary urban locations (“UHII”) or averaged “Top X” warmest grid point values (e.g., “Top 10”, “Top 100”, etc.), a more precise value can be determined from using more information provided from the model simulations. The results for the 21 June 2008 case study (Fig. 31b) show an urban heat island index of approximately 3.3°C to 3.8°C in 2011. The difference between each of the “top X locations” varied more in the 1920 and 1950 runs due to the small number of urban grid spaces being less that some of the calculated thresholds. By

2011, there are more than 1000 grid spaces of urban categories, which leads to the smaller variation in urban heat island index values between the calculations.

Results from the 1 August 2008 (Figs. 32a & 32b), 5 September 2008 (Figs. 33a & 33b), 15 September 2008 (Figs. 34a & 34b), and 15 March 2009 (Figs. 35a & 35b) show similar results. The 1 August 2008 case had urban heat island index values in 2011 from just below 3.0°C to just under 3.5°C and each of the tridecadal values were much closer to each other likely due to the warmer higher terrain being part of the calculation before the urban areas dominate the later runs. The 5 September 2008 and 15 September 2008 cases were very similar in pattern and magnitude to the 21 June 2008 case. The 15 March 2009 case showed dramatic improvements in the calculation of the UHII values using this methodology rather than the standard arbitrary point method. In this case, the arbitrary point method actually has a decreasing urban heat island index from 1.6°C in 1890 to just above 1.0°C in 2011 due to the poor urban air temperature calculations from the WRF in cold weather cases. However, analyzing the warmest point shows a steady increase of UHII values of about 1.0°C over time through its use of the values from within the city boundaries but outside the unresolved portions of the urban core. Overall, this new approach to the calculation of UHII from quantities of grid space values provides more accurate representations of UHII especially in cases where microscale features and/or advection of air temperature may displace the warmest temperatures away from the arbitrary locations.

2 m Air Temperature Coverage Percentile Increases

The urban heat island index, regardless of its method of calculation, provides a single number to indicate maximum value of urban impact to near surface air temperatures; however, it can only be realistically applied to one location, mainly the urban core of a city. Those not living in the maximum urban air temperature locations used in the urban heat island index formula typically do not have an understanding of the urban impacts in their area. This study utilized a new approach to quantify the areal extent of urban heat growth over time through the use of coverage percentiles of specific air temperature values across the domain. By calculating the spatial impacts of increasing air temperatures, a more accurate representation of the urban land use changes with respect to spatial coverage can be presented.

For each of the case studies, the distribution of air temperature values from each of the model output grid points were calculated across the domain for each of the historical periods. Figure 36 shows the categorical air temperature at 02 UTC increase for the 21 June 2008 case study and display the spatial coverage of warming air temperatures as it increased over time. In 1890, 0% of the domain had temperatures at or above 26°C, but by 2011 nearly 20% of the area reached or surpassed this threshold due to the increasing urban impacts. For the 25.5°C threshold, there was an increase of about 23% over the 120 years and an increase of about 28% for the 25.0°C threshold.

Results from the 1 August 2008 at 06 UTC (Fig. 37), 5 September 2008 at 02 UTC (Fig. 38), 15 September 2008 at 02 UTC (Fig. 39), and 15 March 2009 at 03 UTC (Fig. 40) show similar results. The most dramatic increase in the areal coverage of specific urban heat values in each of the graphs occurred between 1950 and 1980, which

corresponds to the largest spatial expansion of urban land use in the study. These results indicate the spatial extent to which the urban land use changes impact the metropolitan areas. Changes in an urban heat island index can indicate the maximum magnitude impacts, while changes in the spatial coverage of temperature thresholds utilizing this unique methodology can indicate areal impacts from urban growth.

2 m Air Temperature Distribution Shift

The spatial air temperature distribution data from the WRF model output can also be utilized to indicate how the temperatures are shifting to warmer values. As a result of the uniqueness of this study in its utilization of historical urban characteristics and large quantity of air temperature values from model simulation grid spaces, histograms of air temperature values at each of the model output grid spaces for each of the case studies were generated and categorized by each of the tridecadal time periods. The values are not cumulative (e.g., "greater than or equal to x°C"), but a count of the values between the value (e.g., x°C) and its next highest categories (e.g., (x+0.5)°C).

For the 21 June 2008 at 02 UTC case study (Fig. 41a), the 23.5°C value was most frequent across the domain in 1890. However, by 2011, the most frequent temperature value has shifted 2.0°C warmer to 25.5°C. Analyzing each individual tridecadal time period shows a transition more towards the right side of the histogram indicating warming trends over time. Looking closer at individual air temperatures can show the change of skewness over time. For example, the distribution of 23.5°C temperatures over the tridecadal periods is skewed right indicating a move away from this value, while the

distribution of 26.0°C temperatures over the tridecadal periods is skewed left indicating that this value is more prevalent in 2011 than in 1890.

Additionally, histograms were created of the maximum and minimum temperatures for the 18 to 12 UTC output periods. The histogram of the maximum air temperatures for the 21 June 2008 case study (Fig. 41b) has a very small range of about 2°C likely due to the maximum day time air temperatures' uniform coverage across both urban and rural areas. A comparison of the minimum air temperatures (Fig. 41c) also indicates the strong warming trend over time with values on the right (e.g., warmer) side of the histogram becoming more frequent over time.

Results from the 1 August 2008 (Figs. 42a, 42b, and 42c), 5 September 2008 (Figs. 43a, 43b, and 43c), 15 September 2008 (Figs. 44a, 44b, and 44c), and 15 March 2009 (Figs. 45a, 45b, and 45c) show similar results. The 1 August 2008, 5 September 2008, and 15 September 2008 cases showed very large counts in the warmest air temperature values in the 1980 and 2011 simulations for both the analysis time and the minimum air temperatures over the entire run time frame and small ranges of approximately 2°C in the maximum air temperatures. Despite the fact that the cold weather case (i.e. 15 March 2009) did not represent urban heat characteristics well in the spatial maps, it had similar results to the warmer weather case study histograms with skewness shifts from a right skewness in colder temperatures to a left skewness of warmer temperatures. Additionally, it also had a very small range of maximum air temperatures similar to the warm temperature cases. This indicates that this new methodology for indicating the changing trends of temperature distributions over time can be utilized for cases in which traditional spatial methodologies may not be useful (e.g. winter cases). One major difference with

this cold weather case is that the distribution peaks of air temperature for each period did not shift over time, but the range of air temperatures did expand to warmer values going from ranges of 3°C in 1890 to 5°C in 2011.

Chapter 8: Conclusions

This study was designed to determine the urban impacts of a developing metropolitan area to the near surface meteorological conditions. Oklahoma City was selected as the research location due to its short historical time frame and its location in a relatively flat and consistent surface free from topographical (e.g. mountains, hills, etc.) or hydrological (e.g. ocean, large lakes, etc.) impacts. Many original and/or newly modified methodologies, data sets, and resulting information were created and utilized throughout this research and the flow chart indicating the work flow is shown in Figure 1.

The first part of this research investigated optimal run-time length of the WRF model, an aspect that other urban heat studies did not perform. The results showed that the summer and early fall cases all accurately represented the patterns of the urban heat island from late afternoon to early morning by the WRF model with air temperature values only differing by approximately 1.0°C or less from verification. However, the cold weather case did not simulate the urban impacts well. While the magnitudes of the rural and urban temperature components differed from verification at times, the resulting UHII remained to within about 0.5°C of the verification from surface observing stations. Depending upon the verification time, differing model runs had different magnitudes of error of air temperatures as compared to the verification data with error values ranging from near 0°C to over 5°C. However, overall, the 24 hour run time simulations resulted in the lowest mean error in three of the cases and was within 1.0°C for the other two cases in the variety of scenarios in which the WRF model was run. Those performing numerical simulations of non-operational case studies should generate run time accuracy statistics for their

model configurations before producing model simulations to ensure a run time that produces the most accurate results.

The second part of the research investigated how the near surface air temperatures increased as a result of the changing land use over time. The results of the historical model runs utilizing the changing land use categories clearly showed the increase of the spatial extent and an over 5.0°C magnitude warming of the near surface air temperatures over and around the developed urban areas. From the removal of all urban categories for the 1890 model simulations, the natural background variability of the air temperatures from topographical features were shown to have UHII values on the order of 1-2°C. These values are important in better understanding all components that must be considered in the calculation of urban heat characteristics. Those performing urban heat island analysis from modeled output would benefit greatly by generating background variability fields through the removal of urban land use categories. The use of air temperature difference maps from the natural background aided in a better understanding of the true urban impacts toward air temperature increases. Previous urban heat studies have thoroughly analyzed current urbanization impacts of meteorological conditions in metropolitan areas across the globe, but this research added a historical perspective to those impacts that was never before shown. City planners and policy decision makers can now understand the magnitude of urban heat impacts that may occur as a result of urban development decisions that are made in the future.

The final section of the research demonstrated additional methodologies for portraying and describing the urban heat island impacts beyond standard heat island indices. One must take careful measures to utilize verification or analysis locations that

best represent the conditions that are occurring. By utilizing the top 10, 100, 500, and 1000 warmest pixels as urban values instead of arbitrary points, a more accurate value for urban heat island indices was calculated (showing value of about 3.5°C in the summer in 2011) because the warmest values for the urban areas were guaranteed to be part of the equation. The distribution of air temperature values from each grid point across the domain for each of the historical time period showed the areal impacts of over 20% in some air temperature thresholds from urban growth, which cannot be gathered from UHIIs which simply indicate maximum air temperature magnitudes of the urban areas. The use of air temperature histograms (in particular for the minimum temperature) of the model grid point's output showed a transition over time more towards the right indicating a warming trend over time. An analysis and understanding of the minimum air temperatures and their shift towards warmer values is critical as heat advisories and warnings for public health are issued based upon overnight minimum air temperatures. Warm, minimum air temperatures overnight impact the human body by not allowing it to cool sufficiently and can lead to heat related illness as a result during prolonged warming periods (Tan et al., 2010). Each of these three unique alternate methodologies aided greatly in better understanding the urban impacts historically, quantitatively, and spatially to the increase in near surface air temperature values from the development of a metropolitan area. While this work was done in the Oklahoma City area, which has fairly flat topographical features and minor hydrological features, these new methodologies could be applied in regions with a more diverse area with topographical and hydrological influences to determine their robustness and applicability.

Overall, through the use of altered land use backgrounds ingested into the WRF model, the results showed that the changes resulting from increased intensity and spatial coverage of the growth of Oklahoma City led to increases in the magnitude and spatial coverage of near surface air temperature values. These results aided in a more comprehensive understanding of potential conditions for growing, existing, and future cities. Additionally, the effectiveness and application of the alternate urban heat island characteristics methodologies presented in this study could be easily applied to other urban modeling research. As more of the world's population continues to either move into urban areas or new urban areas are developed, it is critical to the productivity of its industries, the success of its commercial enterprise, and the health of its residents to understand how the growth of their metropolitan areas impacts their meteorological future.

References

Ackerman, B., 1985: Temporal march of the Chicago heat island, *J. Clim. Appl. Meteor.*, **24**, 547-554.

Adebayo, Y. R., 1987. A note on the effect of urbanization on temperature in Ibadan. *J. of Clim.*, **7**, 185–192.

Aida, M., and K. Gotoh, 1982: Urban albedo as a function of the urban structure—a two-dimensional numerical simulation (part II). *Bound.-Layer Meteor.*, **23**, 415–424.

Alexandri, E. and P. Jones, 2008: Temperature decreases in an urban canyon due to green walls and green roofs in diverse climates. *Building and Environment*, **43**, 480–493. doi: 10.1016/j.buildenv.2006.10.055

Anandakumar, K., 1999: A study on the partition of net radiation into heat fluxes on a dry asphalt surface. *Atmospheric Environment*, **33**, 3911–3918.

Arnfield, A. J., 1990b: Canyon geometry, the urban fabric and nocturnal cooling: a simulation approach. *Physical Geography*, **11**, 220–239.

Arnfield, A. J., 2003: Two decades of urban climate research: a review of turbulence, exchanges of energy and water, and the urban heat island. *Int. J. Climatol.*, **23**, 1–26. doi:10.1002/joc.859

Asaeda, T., V. T. Ca, and A. Wake, 1996: Heat storage of pavement and its effect on the lower atmosphere. *Atmospheric Environment*, **30**, 413–427.

Baik, J., S. Park, and J. Kim, 2009: Urban Flow and Dispersion Simulation Using a CFD Model Coupled to a Mesoscale Model. *J. of Appl. Meteo. and Clim.*, **48**, 1667-1681. doi: 10.1175/2009JAMC2066.1

Bärring, L., J. O. Mattsson, and S. Lindqvist, 1985: Canyon geometry, street temperatures and urban heat island in Malmö, Sweden. *J. of Clim.*, **5**, 433–444.

Basara, J., P. Hall, A. Schroeder, B. Illston, and K. Nemunaitis, 2008: The diurnal cycle of the urban heat island in Oklahoma City, *J. Geophys. Res.*, **113**, D20109, doi:10.1029/2008JD010311.

Basara, J. B., H. G. Basara, B. G. Illston, and K. C. Crawford, 2010: The Impact of the Urban Heat Island during an Intense Heat Wave in Oklahoma City, *Advances in Meteorology*, **230365**, 10 pgs. doi:10.1155/2010/230365

Basara, J. B., B. G. Illston, C. A. Fiebrich, P. D. Browder, C. R. Morgan, A. McCombs, J. P. Bostic, R. A. McPherson, A. J. Schroeder, and K. C. Crawford, 2011: The Oklahoma City Micronet. *Met. Apps*, **18**, 252–261. doi:10.1002/met.189

Brock, F., K. Crawford, R. Elliott, G. Cuperus, S. Stadler, H. Johnson, and M. Eilts, 1995: The Oklahoma Mesonet: a technical overview, *J. Atmos. Oceanic Technol.*, **12**, 5-19.

Brockerhoff, M. P., 2000: An Urbanizing World, *Population Bulletin*, **55**, 3.

Carlson, T. N., J. K. Dodd, S. G. Benjamin, and J. N. Cooper, 1981: Satellite estimation of the surface energy balance, moisture availability and thermal inertia. *Journal of Applied Meteorology*, **20**, 67–87.

Changnon, S. A., 1981: METROMEX: a review and summary. *Meteorological Monographs 18*, **40**.

Changnon S. A., 1992: Inadvertent weather modification in urban areas: lessons for global climate change. *Bull. of the Amer. Meteor. Soc.*, **73**, 619–627.

Chapman, L., J. E. Thornes, and A. V. Bradley, 2001: Rapid determination of canyon geometry parameters for use in surface radiation budgets. *Theor. and Appl. Clim.*, **69**, 81–89.

Chen, F., K. W. Manning, M. A. LeMone, S. B. Trier, J. G. Alfieri, R. Roberts, M. Tewari, D. Niyogi, T. W. Horst, S. P. Oncley, J. B. Basara, and P. D. Blanken, 2007: Description and evaluation of the characteristics of the NCAR High-Resolution Land Data Assimilation System. *J. Appl. Meteor. Climatol.*, **46**, 694-713.

Cionco, R. M., and R. Ellefsen, 1998: High resolution urban morphology data for urban wind flow modeling. *Atmos. Envir.*, **32**, 7–17.

Cohen, J. E., 2003: Human Population: The Next Half Century, *Science*, **302**, 1172-1175.

Cohen, J. E., 2005: Human Population: History, Status, Trends, Presentation at Scientific American & Earth Institute at Columbia University, October 20, 2005.

Dabberdt, W., A. Crook, C. Mueller, J. Hales, S. Zubrick, W. Krajewski, J. C. Doran, C. King, R. N. Keener, R. Bornstein, D. Rodenhuis, P. Kocin, M. A. Rossetti, F. Sharrocks, and E. M. Stanley, 2000: Forecast Issues in the Urban Zone: Report of the 10th Prospectus Development Team of the U.S. Weather Research Program, *Bull. Amer. Meteor. Soc.*, **81**, 2047-2064.

Eliasson, I., 1994: Urban–suburban–rural air temperature differences related to street geometry. *Phys.Geog.*, **15**, 1–22.

Eliasson I., 1996a: Urban nocturnal temperatures, street geometry and land use. *Atmos. Environ.*, **30**, 379–392.

Eliasson I., 1996b: Intra-urban nocturnal temperature differences: a multivariate approach. *Clim. Res.*, **7**, 21–30.

Figuerola, P. I., and N. A. Mazzeo, 1998: Urban–rural temperature differences in Buenos Aires. *Intl. J. of Clim.*, **18**, 1709–1723.

Frank, R. S., R. B. Gerding, P.A. O'Rourke, and W. H. Terjung, 1981b: An urban radiation obstruction model. *Bound.-Layer Meteor.*, **20**, 259–264.

Giannaros, T. M., D. Melas, I. A. Daglis, I. Keramitsoglou, and K. Kourtidis, 2013: Numerical study of the urban heat island over Athens (Greece) with the WRF model. *Atmos. Envir.*, **73**, 103-11. Doi: 10.1016/j.atmosenv.2013.02.055

Grimmond, C. S. B., and T. R. Oke, 1986: Urban water balance. 2. Results from a suburb of Vancouver, British Columbia. *Water Resources Research*, **22**, 1404–1412.

Grimmond, C. S. B., and T. R. Oke, 1999a: Aerodynamic properties of urban areas derived from analysis of surface form. *J. of Appl. Meteor.*, **38**, 1262–1292.

Grimmond, C. S. B., and T. R. Oke, 1999b. Heat storage in urban areas: local-scale observations and evaluation of a simple model. *J. of Appl. Meteor.*, **38**, 922–940.

Grimmond, C. S. B., T. R. Oke, and D. G. Steyn, 1986: Urban water balance. 1. A model for daily totals. *Water Resources Research*, **22**, 1397–1403.

Grimmond, C. S. B., H. A. Cleugh, and T. R. Oke, 1991: An objective urban heat storage model and its comparison with other schemes. *Atmospheric Environment B*, **25**, 311–326.

Grimmond, C. S. B., C. Souch, and M. D. Hubble, 1996: Influence of tree cover on summertime surface energy balance fluxes, San Gabriel Valley, Los Angeles. *Clim. Res.*, **6**, 45–57.

Grimmond, C. S. B., T. S. King, M. Roth, and T. R. Oke, 1998: Aerodynamic roughness of urban areas derived from wind observations. *Bound.-Layer Meteor.*, **89**, 1–24.

Hafner, J., and S. Q. Kidder, 1999: Urban heat island modeling in conjunction with satellite-derived surface/soil parameters. *J. of Appl. Meteor.*, **38**, 448–465.

Hawkins, T., A. Brazel, W. Stefanov, W. Bigler, and E. Saffell, 2004: The role of rural variability in Urban Heat Island Determination for Phoenix, Arizona, *J. Appl. Meteor*., **43,** 476-486.

Herbert, J. M., G. T. Johnson, and A. J. Arnfield, 1998: Modelling the thermal climate in city canyons. *Environmental Modelling and Software*, **13**, 267–277.

Hildebrand, P. H., and B. Ackerman, 1984: Urban effects on the convective boundary

layer. *J. of the Atmos. Sci.*, **41**, 76–91.

Jauregui, E., 1997: Heat island development in Mexico City. *Atmospheric Environment*, **31**, 3821–3831.

Johnson, D. B., 1985: Urban modification of diurnal temperature cycles in Birmingham, U.K. *J. of Clim.*, **5**, 221–225.

Johnson, G.T., and L. J. Hunter, 1995: A numerical study of dispersion of passive scalars in city canyons. *Bound.-Layer Meteor.*, **75**, 209–234.

Jones, C.A., and P. W. Suckling, 1983: Comparison of the radiation balance of a rooftop lawn with that of a conventional rooftop surface. *Archives for Meteor., Geophysics and Bioclimatology B*, **33**, 77–87.

Kim, H. H., 1992: Urban heat island. *Intl. J. of Remote Sensing*, **13**, 2319–2336.

Kim, Y., and J. Baik, 2005: Spatial and temporal structure of the urban heat island in Seoul, *J. Appl. Meteor.*, **44**, 591-605.

Kłysik, K., and K. Fortuniak, 1999: Temporal and spatial characteristics of the urban heat island of Łódź, Poland. *Atmospheric Environment*, **33**, 3885–3895.

Kukla, G., J. Gavin, and T. R. Karl, 1986: Urban warming. *J. of Appl. Meteor.*, **25**, 1265–1270.

Kumar, S., T. Prasad, N. V. Sashidharan, and S. K. Nair, 2001: Heat island intensities over Brihan Mumbai on a cold winter and hot summer night. *Mausam*, **52**, 703–708.

Landsberg, H. E., 1981a: City climate. *General Climatology, 3*, LandsbergHE (ed.). Elsevier Scientific: New York.

Landsberg, H. E., 1981b: *The Urban Climate*. Academic Press: New York.

Lee, K. N., 2009: An Urbanizing World, *Bull. Amer. Meteor. Soc.*, **90**, 441–442.

Li, X., D. Y. C. Leung, and C. Liu, 2007: Physical Modeling of Flow Field inside Urban Street Canyons, *J. of Appl. Meteor. and Clim.*, **47**, 2058-2067. DOI: 10.1175/2007JAMC1815.1

Lin, C.-Y., F. Chen, J. C. Huang, W.-C. Chen, Y.-A. Liou, W.-N. Chen, and S.-C. Liu, 2008: Urban heat island effect and its impact on boundary layer development and land–sea circulation over northern Taiwan. *Atmos. Envir.*, **42**, 5635-5649. doi: 10.1016/j.atmosenv.2008.03.015

Magee, N., J. Curtis, and G. Wendler, 1999: The urban heat island effect at Fairbanks, Alaska. *Theoretical and Appl. Clim.*, **64**, 39–47.

McPherson, R. A., C. Fiebrich, K. C. Crawford, R. L. Elliott, J. R. Kilby, D. L. Grimsley, J. E. Martinez, J. B. Basara, B. G. Illston, D. A. Morris, K. A. Kloesel, S. J. Stadler, A. D. Melvin, A.J. Sutherland, and H. Shrivastava, 2007: Statewide monitoring of the mesoscale environment: A technical update on the Oklahoma Mesonet. *J. Atmos. Oceanic Tech.*, **24**, 301-321.

Mesinger, F., G. DiMego, E. Kalnay, K. Mitchell, P. C. Shafran, W. Ebisuzaki, D. Jovic, J. Woollen, E. Rodgers, E. H. Berbery, M. B. Ek, Y. Fan, R. Grumbine, W. Higgins, H. Li, Y. Lin, G. Manikin, D. Parrish, and W. Shi, 2006: North American Regional Reanalysis. *Bull. Amer. Meteor. Soc.*, **87**, 343-360. DOI: 10.1175/BAMS-87-3-343.

Meyn, S. K., and T. R. Oke, 2009: Heat fluxes through roofs and their relevance to estimates of urban heat storage. *Energy and Buildings*, **41**, 745–752. DOI: 10.1016/j.enbuild.2009.02.005.

Miao, S., F. Chen, M. A. LeMone, M. Tewari, Q. Li, and Y. Wang, 2009: An Observational and Modeling Study of Characteristics of Urban Heat Island and Boundary Layer Structures in Beijing. *J. Appl. Meteor. Climatol.*, **48**, 484–501, doi: 10.1175/2008JAMC1909.1.

Mitchell, V. G., H. A. Cleugh, C. S. B. Grimmond, and J. Xu, 2008: Linking urban water balance and energy balance models to analyse urban design options. *Hydrol. Process*., **22**, 2891-2900. DOI: 10.1002/hyp.6868

Moreno-Garcia, M. C., 1994: Intensity and form of the urban heat island in Barcelona. *Intl. J. of Clim.*, **14**, 705–710.

Morris, C. J. G., and I. Simmonds, 2000: Associations between varying magnitudes of the urban heat island and the synoptic climatology in Melbourne, Australia. *Intl. J. of Clim.*, **20**, 1931–1954.

Nasrallah, H. A., A. J. Brazel, and R. C. Balling, 1990: Analysis of the Kuwait City urban heat island. *Intl. J. of Clim.*, **10**, 401–405.

Nemunaitis, K. L., 2014: Observational and Model Analyses of the Oklahoma City Urban Heat Island, Ph. D. Dissertation, School of Meteorology, University of Oklahoma, Norman, 223 pp..

Oke, T. R., 1974: Review of Urban Climatology, 1968–1973. WMO Technical Note No. 134, WMO No. 383. World Meteorological Organization: Geneva.

Oke, T. R., 1979b: *Review of Urban Climatology, 1973–1976*. WMO Technical Note No. 169, WMo No. 539. World Meteorological Organization: Geneva.

Oke, T. R., 1980: *Bibliography of Urban Climate, 1977–1980*. World Climate Program Publication 45. World Meteorological Organization: Geneva.

Oke, T. R., 1981: Canyon geometry and the nocturnal heat island: comparison of scale model and field observations. *J. of Clim.*, **1**, 237–254.

Oke, T. R., 1987: *Boundary Layer Climates*, Routledge, 435 pp.

Pan, H.-L., and L. Mahrt, 1987: Interaction between soil hydrology and boundary layer development. *Bound.-Layer Meteor.*, **38**, 185-202.

Park, H. S., 1986: Features of the heat island in Seoul and its surrounding cities. *Atmospheric Environment*, **20**, 1859–1866.

Richiardone, R., and G. Brusasca, 1989: Numerical experiments on urban heat island intensity. *Quarterly J. of the Royal Meteor. Soc.*, **115**, 983–995.

Runnals, K. E., and T. R. Oke, 2000: Dynamics and controls of the near-surface heat island of Vancouver, British Columbia. *Phys. Geog.*, **21**, 283–304.

Sakakibara, Y., 1996: A numerical study of the effect of urban geometry upon the surface energy budget. *Atmospheric Environment*, **30**, 487–496.

Salamanca, F., A. Martilli, and C. Yagüe, 2012: A numerical study of the Urban Heat Island over Madrid during the DESIREX (2008) campaign with WRF and an evaluation of simple mitigation strategies. *Int. J. Climatol.*, **32**, 2372–2386. doi:10.1002/joc.3398

Schmidlin, T. W., 1989: The urban heat island at Toledo, Ohio. *Ohio J. of Science*, **89**, 38–41.

Schroeder, A. J., J. B. Basara, and B. G. Illston, 2010: Challenges Associated with Classifying Urban Meteorological Stations: The Oklahoma City Micronet Example, *The Open Atmospheric Science Journal*, **4**, 88-100.

Shafer, M., C. Fiebrich, D. Arndt, S. Fredrickson, and T. Hughes, 2000: Quality assurance procedures in the Oklahoma Mesonet, *J. Atmos. Oceanic Tech.*, **17**, 474-494.

Shahgedanova, M., T. P. Burt, and T. D. Davies, 1997: Some aspects of the three-dimensional heat island in Moscow. *Intl. J. of Clim.*, **17**, 1451–1465.

Sievers, U., and W. Zdunkowski, 1985: A numerical simulation scheme for the albedo of city street canyons. *Bound.-Layer Meteor.*, **33**, 245–257.

Swaid, H., and M. E. Hoffman, 1990–91: Thermal effects of artificial heat sources and shaded ground areas in the urban canopy layer. *Energy and Buildings*, **15–16**, 253–261.

Taha, H., 1997: Urban climates and heat islands: albedo, evapotranspiration, and anthropogenic heat. *Energy and Buildings*, **25**, 99-103.

Tan, J., Y. Zheng, X. Tang, C. Guo, L. Li, G. Song, X. Zhen, D. Yuan, A.J. Kalkstein, F. Li, and H. Chen, 2010: The urban heat island and its impact on heat waves and human health in Shanghai. *Int. J. Biometeorol.*, **54**, 75-84.

Tapper, N. J., 1990: Urban influences on boundary layer temperature and humidity: results from Christchurch, New Zealand. *Atmospheric Environment B*, **24**, 19–27.

Unger, J., 1996: Heat island intensity with different meteorological conditions in a medium-sized town: Szeged, Hungary. *Theoretical and Appl. Clim.*, **54**, 147–151.

Unger, J., Z. Sümeghy, and J. Zoboki, 2001: Temperature cross-section features in an urban area. *Atmos. Res.*, **58**, 117–127.

United Nations, 2000: Charting the Progress of Populations, UN Sales Number E.00.XIII.6 (paper). 95pgs.

United Nations, 2003: World Urbanization Prospects – 2003 Revision, Online available at www.unpopulation.org.

United Nations, 2009: World Urbanization Prospects: The 2007 Revision Population Database. Online available at http://esa.un.org/unup/.

United States Census Bureau, 2004: Global Population at a Glance: 2002 and Beyond, *International Population Reports*, 1-4.

United States Census Bureau, 2009: Metropolitan and micropolitan statistical area population and estimated components of change: April 1, 2000 to July 1, 2008. Online available at http://www.census.gov/popest/metro/files/2008/CBSA-EST2008-alldata.csv.

United States Census Bureau, 2009: Annual Estimates of the Resident Population for Incorporated Places Over 100,000. Online available at http://www.census.gov/popest/cities/tables/SUB-EST2008-01.csv.

Voogt, J. A., and C. S. B. Grimmond, 2000: Modeling surface sensible heat flux using surface radiative temperatures in a simple urban area. *J. of Appl. Meteor.*, **39**, 1679–1699.

Wang, C., and J. Liu, 1982: The climate of the City of Hangzhou. *Acta Geographica Sinica*, **37**, 164–173.

Wang, J., T. A. Endreny, and D. J. Nowak, 2008: Mechanistic Simulation of Tree Effects in an Urban Water Balance Model. *J. of the Amer. Water Res. Assoc.*, **44**, 75–85. DOI:10.1111/j.1752-1688.2007.00139.x

World Meteorological Organization, 1983: Guide to Meteorological Instruments and Methods of Observation. 5th ed. WMO 8, Geneva, Switzerland.

Yagüe, C., E. Zurita, and A. Martinez, 1991: Statistical analysis of the Madrid urban heat island. *Atmospheric Environment B*, **25**, 327–332.

Appendix A: Tables

Date	Urban Temperature (°C)	Rural Temperature (°C)	UHII (°C)	Avg. 2 m Wind Speed (m/s)
21 June 2008	23.3	20.0	3.3	0.0
01 August 2008	25.9	22.9	3.0	0.8
05 September 2008	17.6	14.6	3.0	0.0
15 September 2008	13.8	9.4	4.4	1.2
15 March 2009	6.3	3.0	3.3	0.2

Table 1. A list of candidate days indicating their season and their meteorological conditions at 12 UTC. Urban/Rural temperatures are an average of the temperatures measured from Oklahoma City Micronet Central Business District stations (e.g. urban) and Oklahoma Mesonet stations surrounding the Oklahoma City area (e.g. "rural"). The urban heat island index is the difference between the urban and rural averaged temperatures.

Option	Value	Value Description
Time Control		
Run Hours	Var.	Run time in hours
Start Hour	Var.	UTC hour of start time
Interval Seconds	10800	Time interval between incoming real data, which will be the interval between the lateral boundary conditions file
Time Step	3	Time step integration in seconds
Domain		
Metgrid Levels	40	Number of vertical levels
Eta Levels	TBD	Model Eta levels
Top Pressure Level	5000	Top pressure level in pascals
Physics		
Microphysics	6	WSM 6-class graupel scheme
Longwave Radiation	1	Rrtm scheme
Shortwave Radiation	1	Dudhia scheme
Surface Layer Physics	1	Monin-Obukhov scheme
Land-Surface Option	2	Unified Noah land-surface model
PBL Physics	1	YSU scheme
Cumulus Options	0	No cumulus
Heat and Moisture Fluxes	1	With fluxes from the surface
Num Soil Layers	4	Noah land-surface model
Urban Canopy Model	1	Activated in Noah LSM
Dynamics		
Time Integration	3	Runge-Kutta 3rd order
Turbulence and Mixing	1	Evaluates 2nd order diffusion term on coordinate surfaces
Eddy Coefficient	4	Horizontal Smagorinsky first order closure
Upper Level Damping	0	No upper level damping
Non-hydrostatic	true	Running in non-hydrostatic mode

Table 2. A list of WRF/WPS options selected for all model runs.

		18hr	24hr	30hr	36hr	42hr	48hr
Urban	Validation Time	0.66	0.37	0.13	0.21	-0.36	0.05
	±1 hr	0.67	0.39	0.27	0.29	-0.37	-0.02
	All Times	-0.04	0.11	-0.15	0.01	-0.77	-0.36
Rural	Validation Time	2.03	1.41	1.53	2.36	1.16	1.35
	±1 hr	1.80	1.07	1.17	1.90	0.81	1.01
	All Times	1.28	0.73	0.48	0.98	-0.05	0.06
UHII	Validation Time	-1.37	-1.04	-1.40	-2.15	-1.51	-1.31
	±1 hr	-1.12	-0.68	-0.91	-1.62	-1.18	-1.03
	All Times	-1.32	-0.63	-0.64	-0.97	-0.72	-0.42

Table 3. Mean errors in air temperature in model simulations of 02 UTC ("Validation Time"), 01-03 UTC ("±1 hr"), and the 18 hours ending at 12 UTC ("All Times") for the 21 June 2008 case.

		18hr	24hr	30hr	36hr	42hr	48hr
Urban	Validation Time	1.14	0.97	0.94	0.45	0.96	-1.12
	±1 hr	0.87	0.82	0.98	0.55	0.97	-1.09
	All Times	1.45	1.23	1.17	0.98	1.68	-0.40
Rural	Validation Time	1.84	1.78	1.66	1.32	0.99	-0.41
	±1 hr	1.87	1.72	1.76	1.33	1.01	-0.37
	All Times	1.89	1.65	1.47	1.29	1.59	-0.15
UHII	Validation Time	-0.71	-0.80	-0.72	-0.87	-0.02	-0.71
	±1 hr	-1.00	-0.91	-0.78	-0.78	-0.04	-0.72
	All Times	-0.45	-0.42	-0.30	-0.31	0.09	-0.25

Table 4. Mean errors in air temperature in model simulations of 06 UTC ("Validation Time"), 05-07 UTC ("±1 hr"), and the 18 hours ending at 12 UTC ("All Times") for the 1 August 2008 case.

		18hr	24hr	30hr	36hr	42hr	48hr
Urban	Validation Time	0.11	-0.43	-0.96	0.02	-0.04	-0.63
	±1 hr	0.52	-0.08	-0.78	0.15	0.12	-0.50
	All Times	0.26	0.22	-1.33	-0.22	-0.62	-1.14
Rural	Validation Time	1.71	0.91	0.73	1.52	0.80	0.29
	±1 hr	1.49	0.79	0.62	1.29	0.67	0.10
	All Times	1.07	0.59	-0.09	0.88	0.31	-0.21
UHII	Validation Time	-1.60	-1.34	-1.68	-1.50	-0.85	-0.92
	±1 hr	-0.98	-0.87	-1.40	-1.13	-0.55	-0.59
	All Times	-0.81	-0.37	-1.25	-1.10	-0.94	-0.93

Table 5. Mean errors in air temperature in model simulations of 02 UTC ("Validation Time"), 01-03 UTC ("±1 hr"), and the 18 hours ending at 12 UTC ("All Times") for the 5 September 2008 case.

		18hr	24hr	30hr	36hr	42hr	48hr
Urban	Validation Time	1.19	1.19	2.22	1.82	2.50	1.82
	±1 hr	1.07	1.01	2.03	1.71	2.35	1.70
	All Times	0.43	0.67	1.49	0.85	1.71	1.45
Rural	Validation Time	2.74	2.35	3.57	3.32	4.02	3.33
	±1 hr	2.45	2.09	3.25	3.08	3.45	2.96
	All Times	1.87	1.69	2.60	2.05	2.65	2.30
UHII	Validation Time	-1.55	-1.16	-1.35	-1.50	-1.52	-1.51
	±1 hr	-1.38	-1.08	-1.22	-1.37	-1.11	-1.25
	All Times	-1.44	-1.01	-1.11	-1.20	-0.94	-0.86

Table 6. Mean errors in air temperature in model simulations of 02 UTC ("Validation Time"), 01-03 UTC ("±1 hr"), and the 18 hours ending at 12 UTC ("All Times") for the 15 September 2008 case.

		18hr	24hr	30hr	36hr	42hr	48hr
Urban	Validation Time	-2.69	-1.84	-1.68	-1.86	-1.75	-2.45
	±1 hr	-2.70	-2.01	-1.77	-1.66	-1.73	-2.32
	All Times	-2.54	-3.44	-1.89	-1.87	-1.91	-2.27
Rural	Validation Time	0.70	0.43	1.15	1.43	1.51	0.91
	±1 hr	0.51	0.33	0.95	1.18	1.21	0.66
	All Times	-0.10	-0.76	0.30	0.52	0.59	0.11
UHII	Validation Time	-3.39	-2.27	-2.83	-3.28	-3.26	-3.36
	±1 hr	-3.20	-2.33	-2.72	-2.84	-2.94	-2.98
	All Times	-2.44	-2.68	-2.19	-2.39	-2.50	-2.38

Table 7. Mean errors in air temperature in model simulations of 03 UTC ("Validation Time"), 02-04 UTC ("±1 hr"), and the 18 hours ending at 12 UTC ("All Times") for the 15 March 2009 case.

Appendix B: Figures

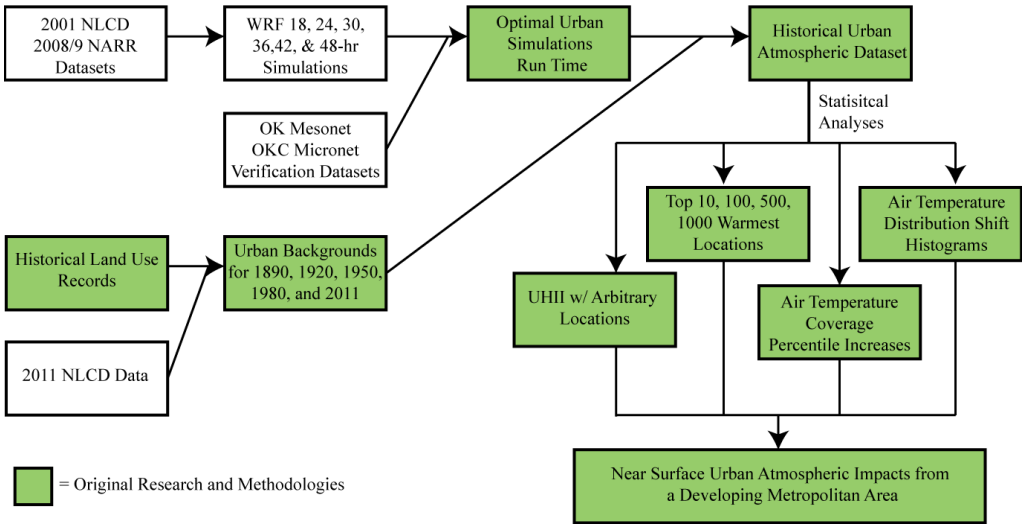

Figure 1. Methodology flow chart of this research study indicating procedures and results of original content and results.

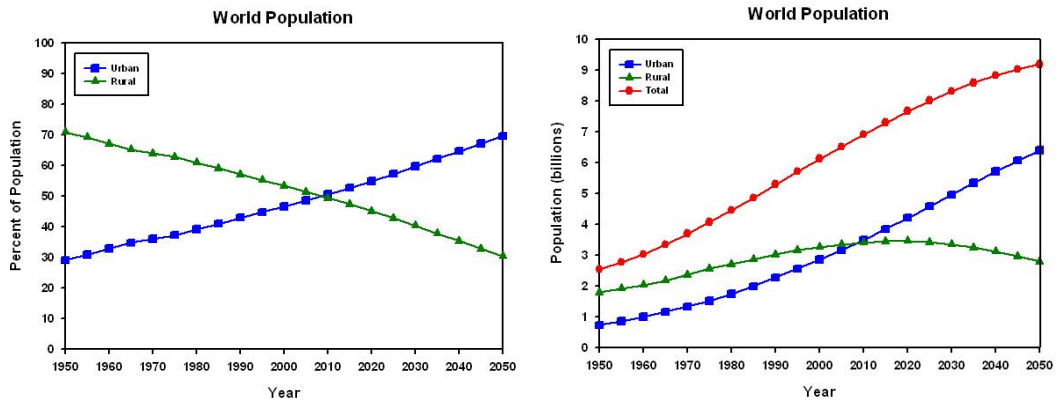

Figure 2. Urban and rural population trends and projections of the world. (United Nations, 2009)

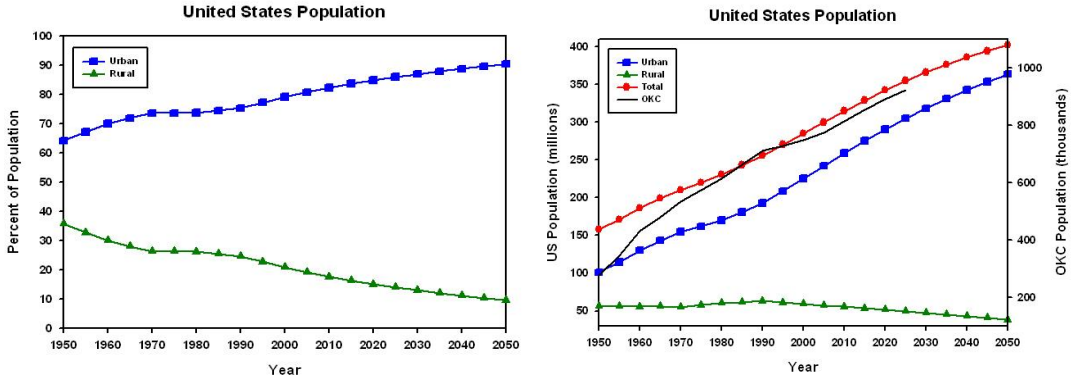

Figure 3. Urban and rural population trends and projections of the United States. (United Nations, 2009)

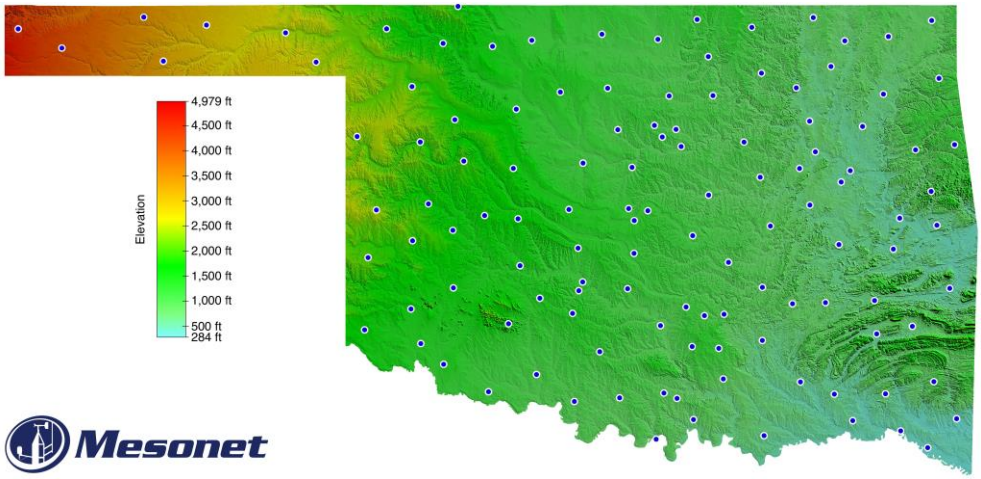

Figure 4. Topographical map of Oklahoma. (Courtesy of Oklahoma Mesonet)

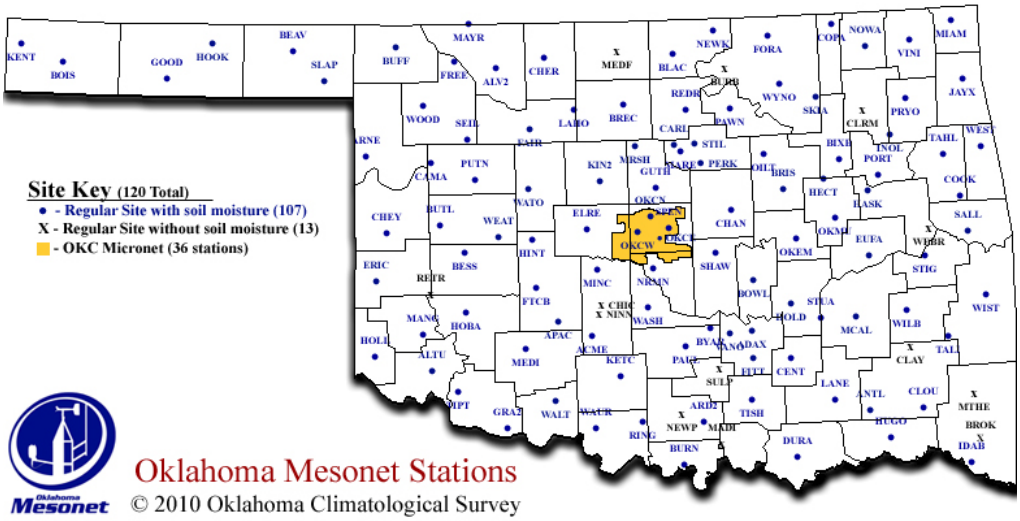

Figure 5. A map of the Oklahoma Mesonet in 2010.

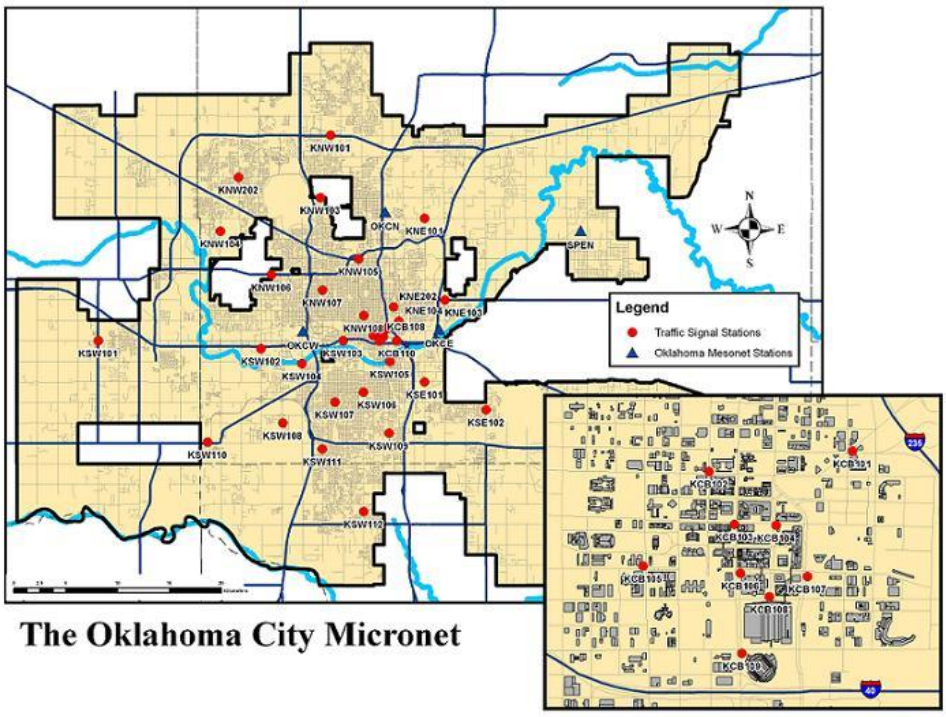

Figure 6. A map of the Oklahoma City Micronet with a Central Business District inset.

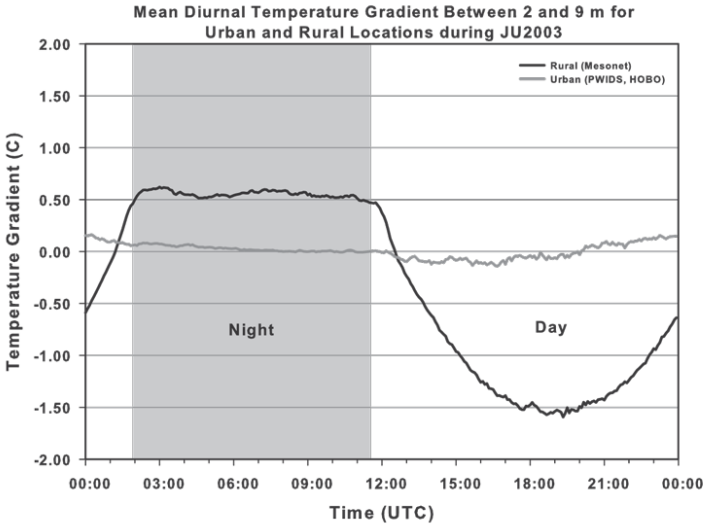

Figure 7. Mean diurnal air temperature gradients between 2 m and 9 m in urban and rural locations during Joint Urban 2003. (Basara et al., 2008)

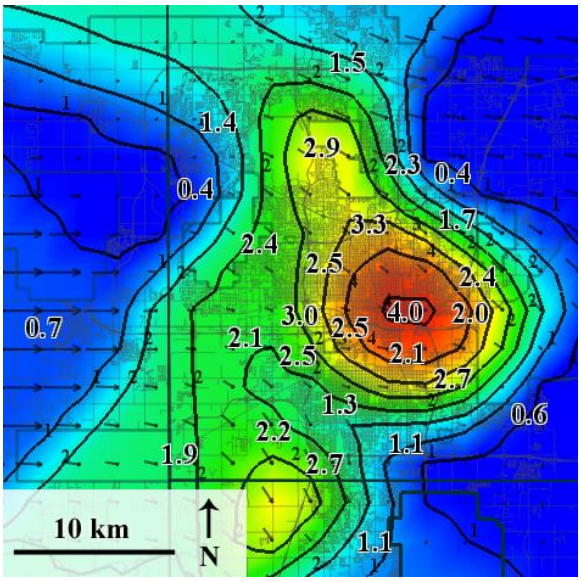

Figure 8. Example of a heat island measured by the Oklahoma City Micronet. (Schroeder et al., 2010).

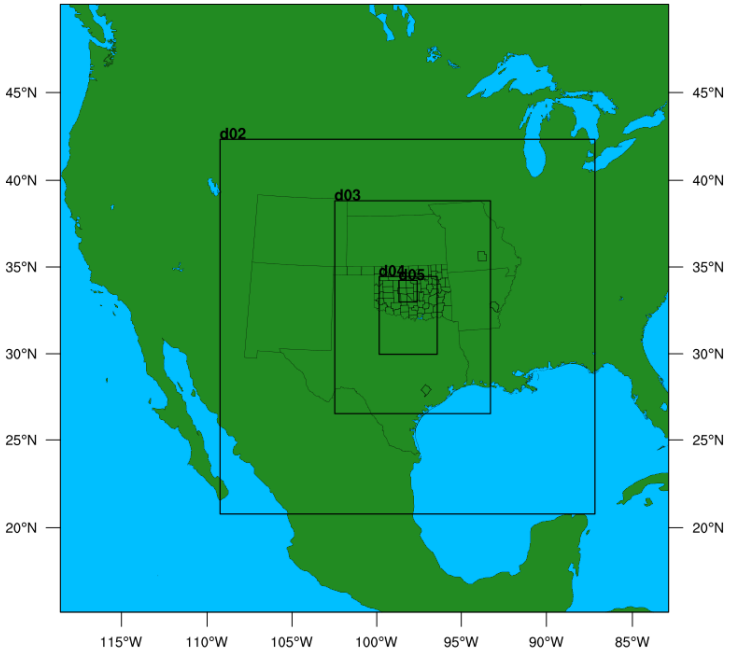

Figure 9. WRF domains: 4050 km x 4050 km with 40.5 km grid spacing (d01), 1350 km x 1350 km with 13.5 km grid spacing (d02), 450 km x 450 km with 4.5 km grid spacing (d03), 150 km x 150 km with 1.5 km grid spacing (d04), and 50 km x 50 km with 500 m grid spacing (d05).

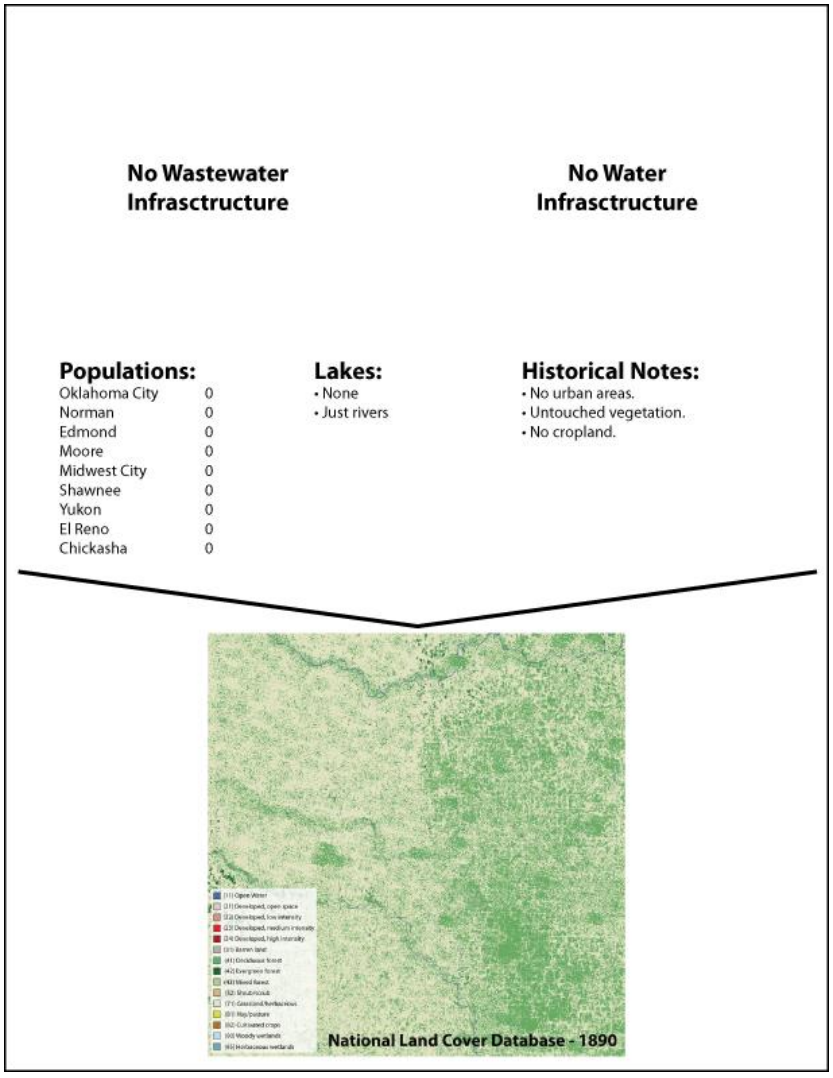

Figure 10. Historical information with which the background land cover images for 1890 were created.

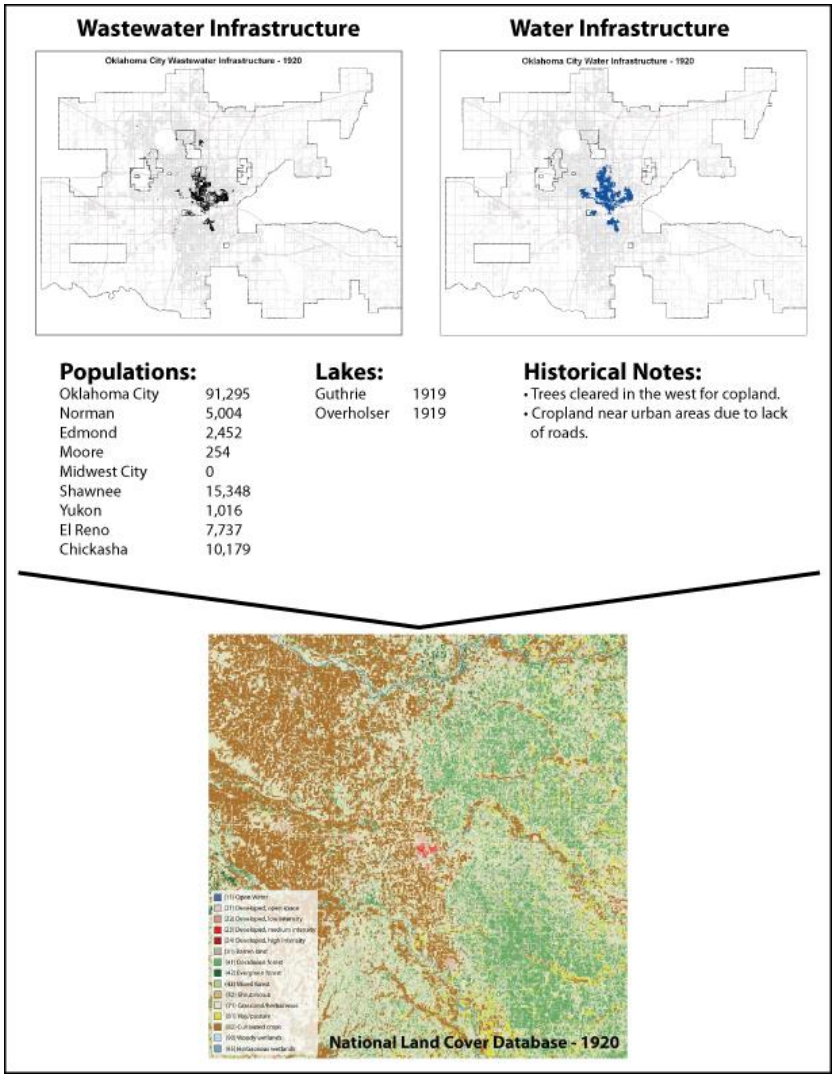

Figure 11. Historical information with which the background land cover images for 1920 were created.

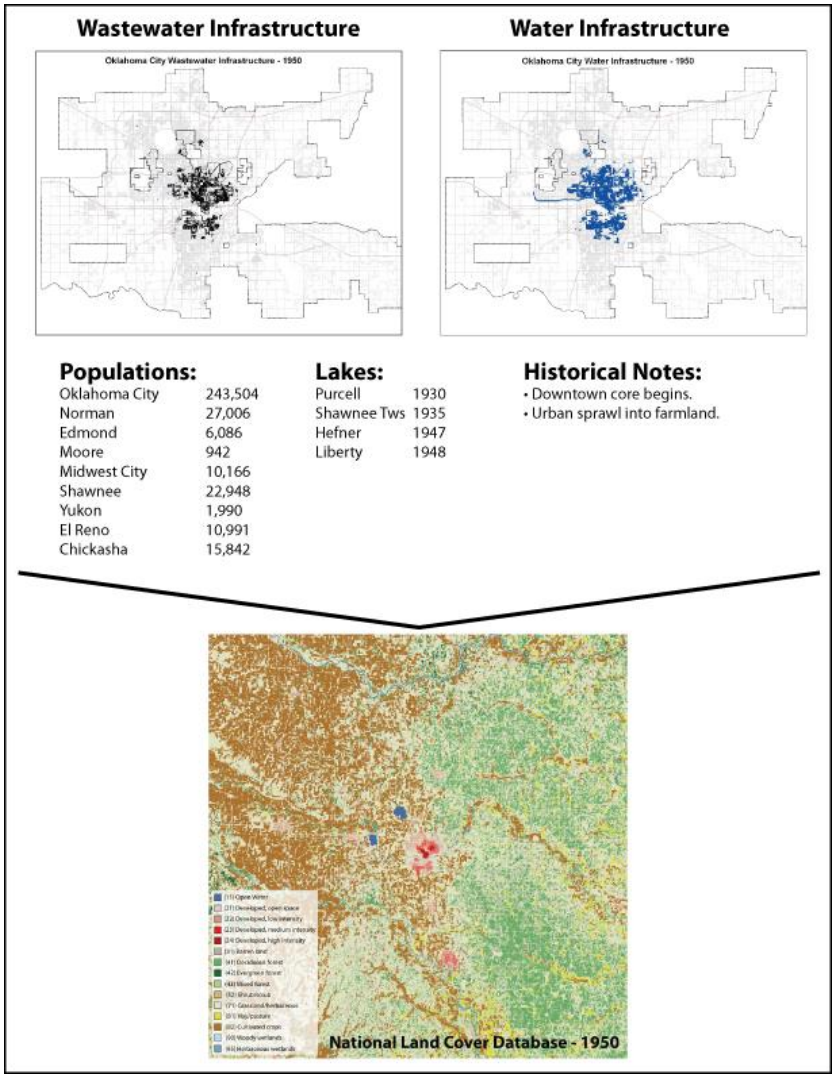

Figure 12. Historical information with which the background land cover images for 1950 were created.

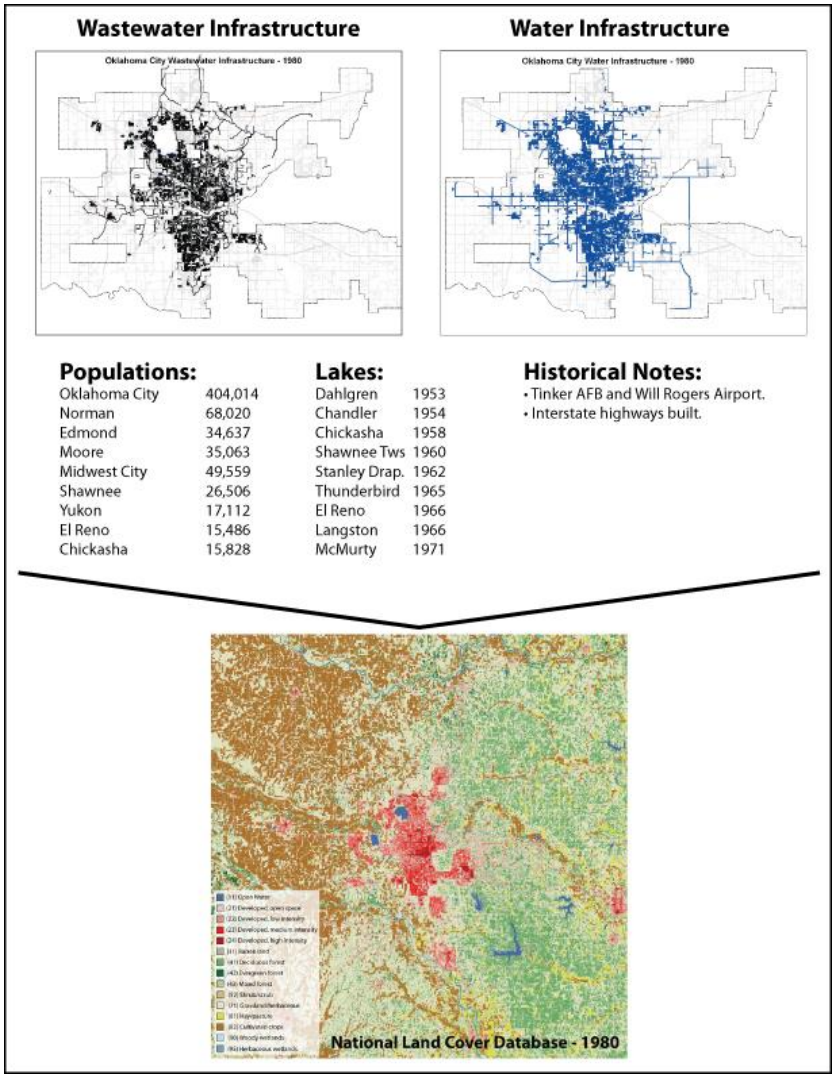

Figure 13. Historical information with which the background land cover images for 1980 were created.

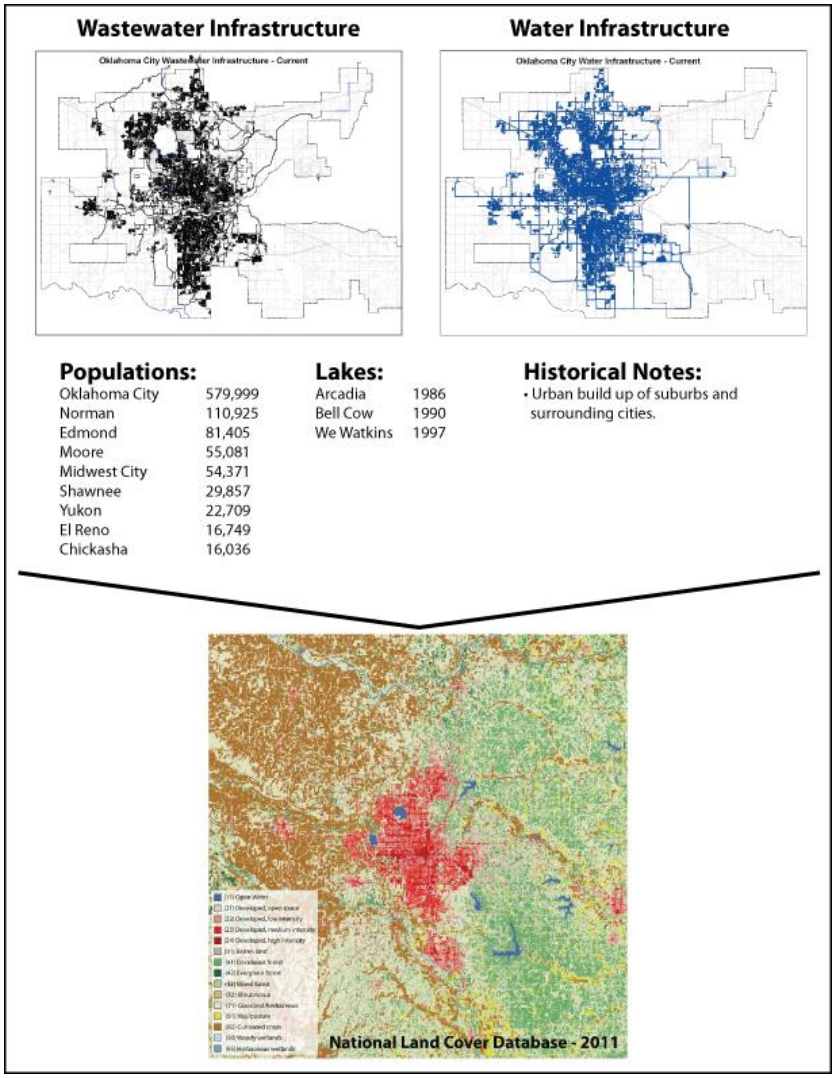

Figure 14. Historical information with which the background land cover images for 2011 were created.

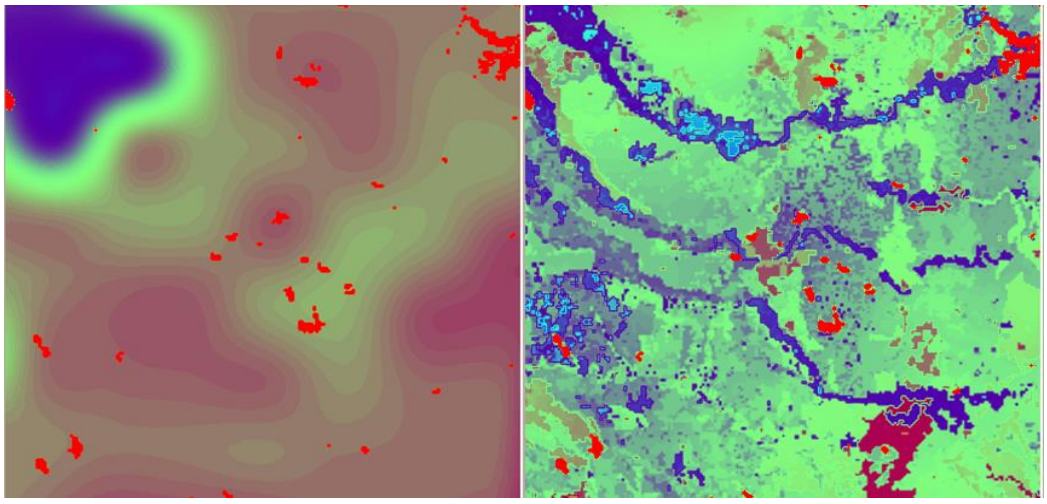

Figure 15. WRF initialization field of soil moisture conditions at a 1-km grid using just NARR initial conditions and no NLDAS spin-up (left) and using a 5-year spin up of NLDAS and NARR initial conditions (right). (Nemunaitis, 2014)

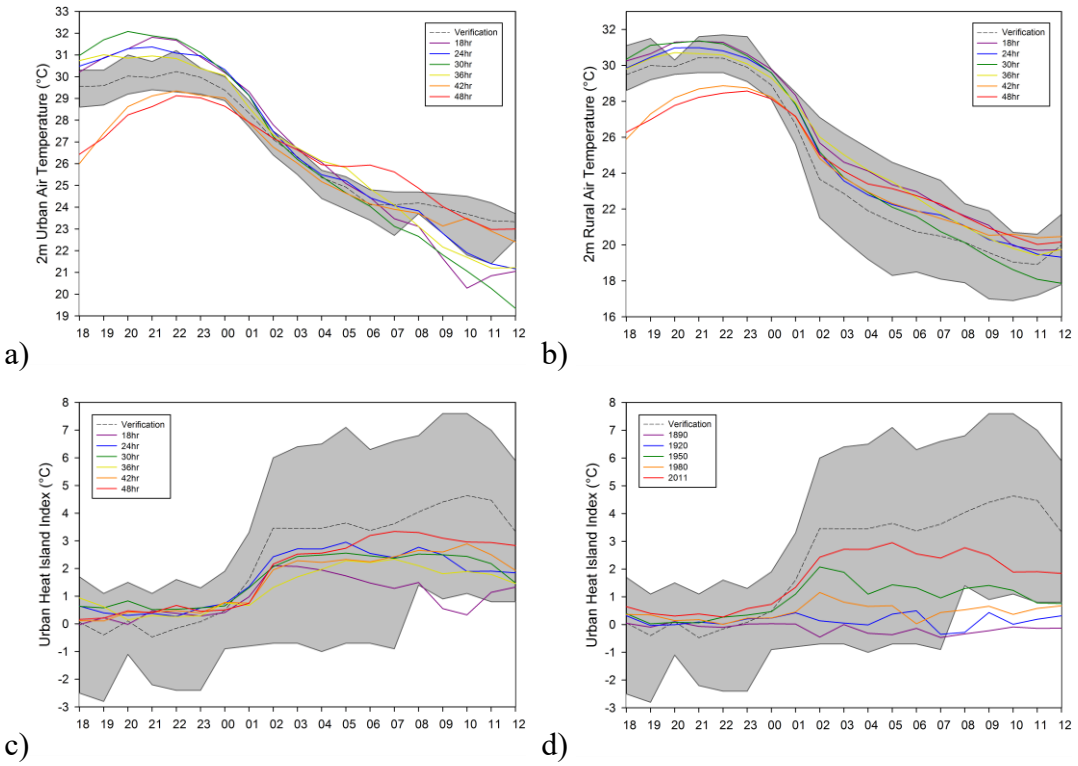

Figure 16. Run time accuracy of air temperature simulations at 2 m for urban stations (a), rural stations (b), and the resulting UHII (c) for 21 June 2008 case study. The simulation comparison of historical 24 hour UHII simulations (d) are also shown.

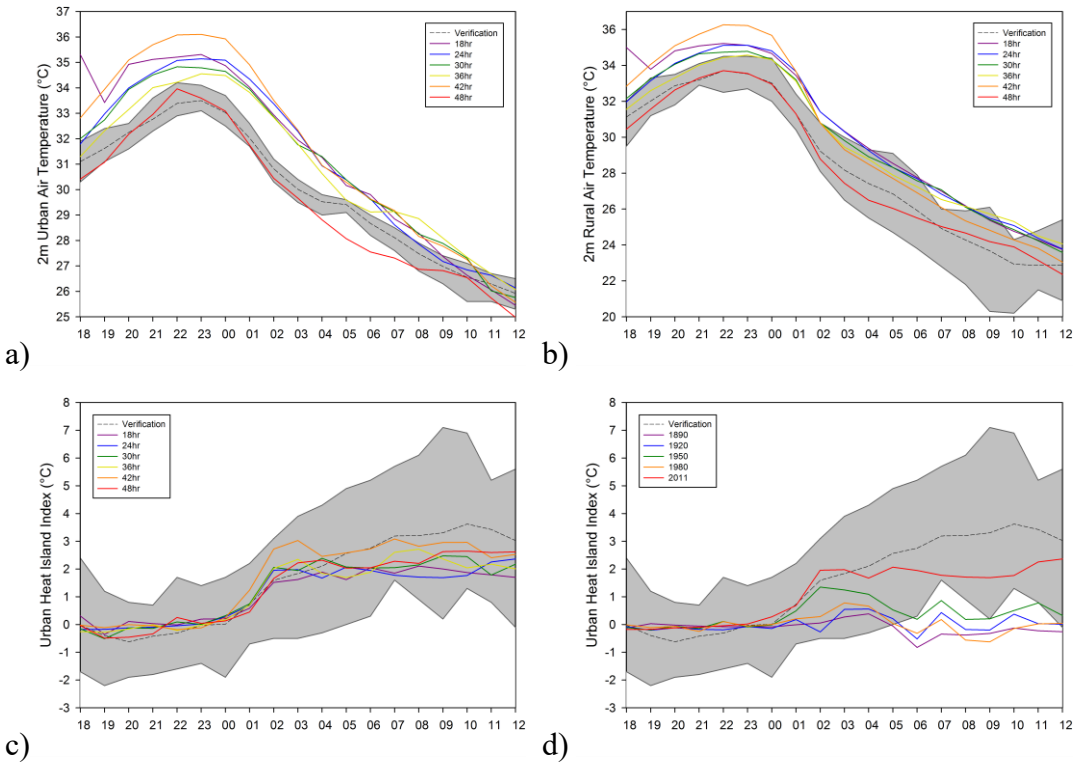

Figure 17. Run time accuracy of air temperature simulations at 2 m for urban stations (a), rural stations (b), and the resulting UHII (c) for 1 August 2008 case study. The simulation comparison of historical 24 hour UHII simulations (d) are also shown.

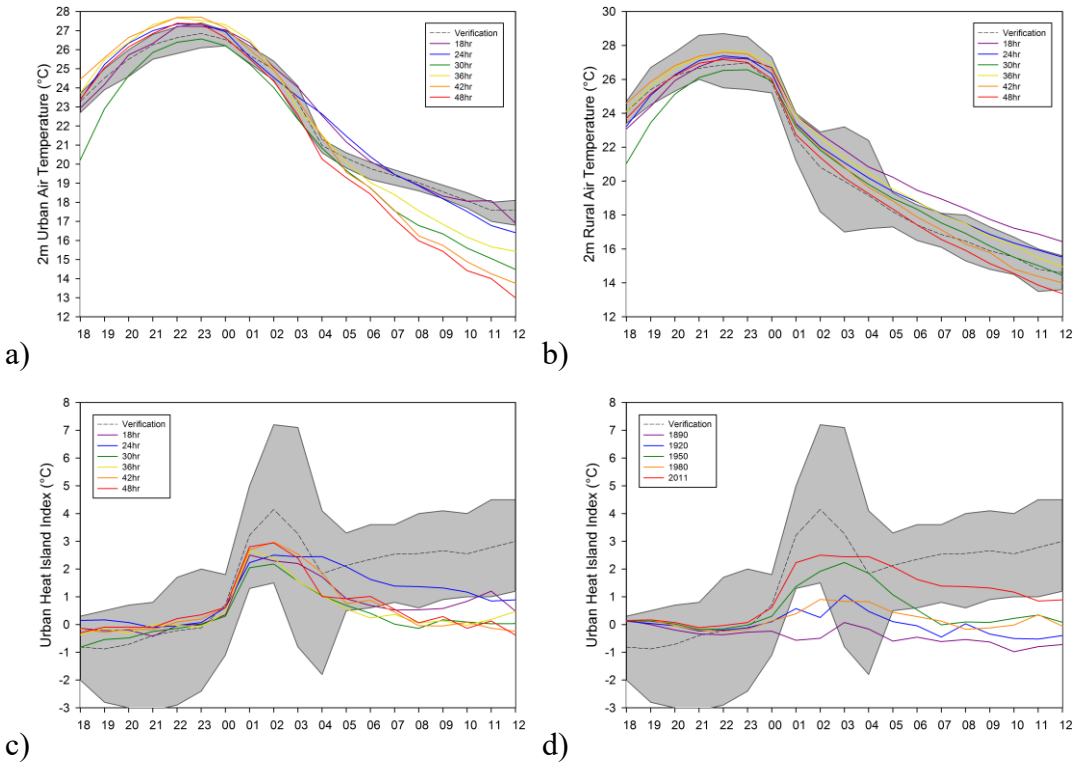

Figure 18. Run time accuracy of air temperature simulations at 2 m for urban stations (a), rural stations (b), and the resulting UHII (c) for 5 September 2008 case study. The simulation comparison of historical 24 hour UHII simulations (d) are also shown.

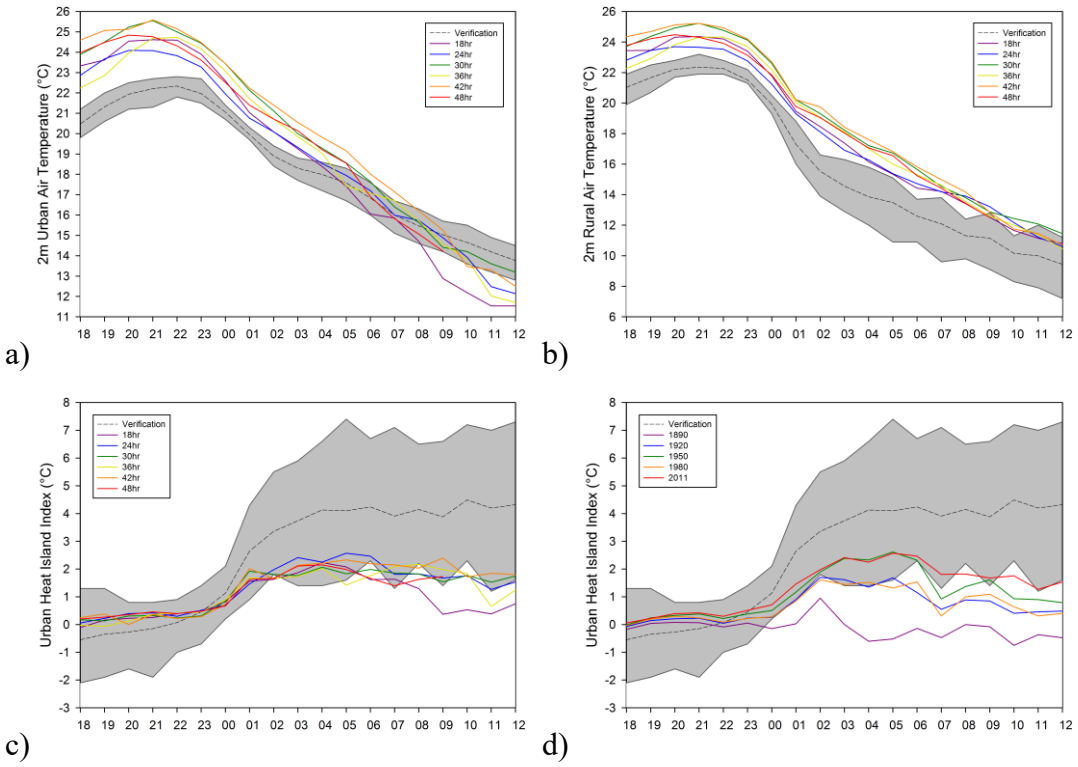

Figure 19. Run time accuracy of air temperature simulations at 2 m for urban stations (a), rural stations (b), and the resulting UHII (c) for 15 September 2008 case study. The simulation comparison of historical 24 hour UHII simulations (d) are also shown.

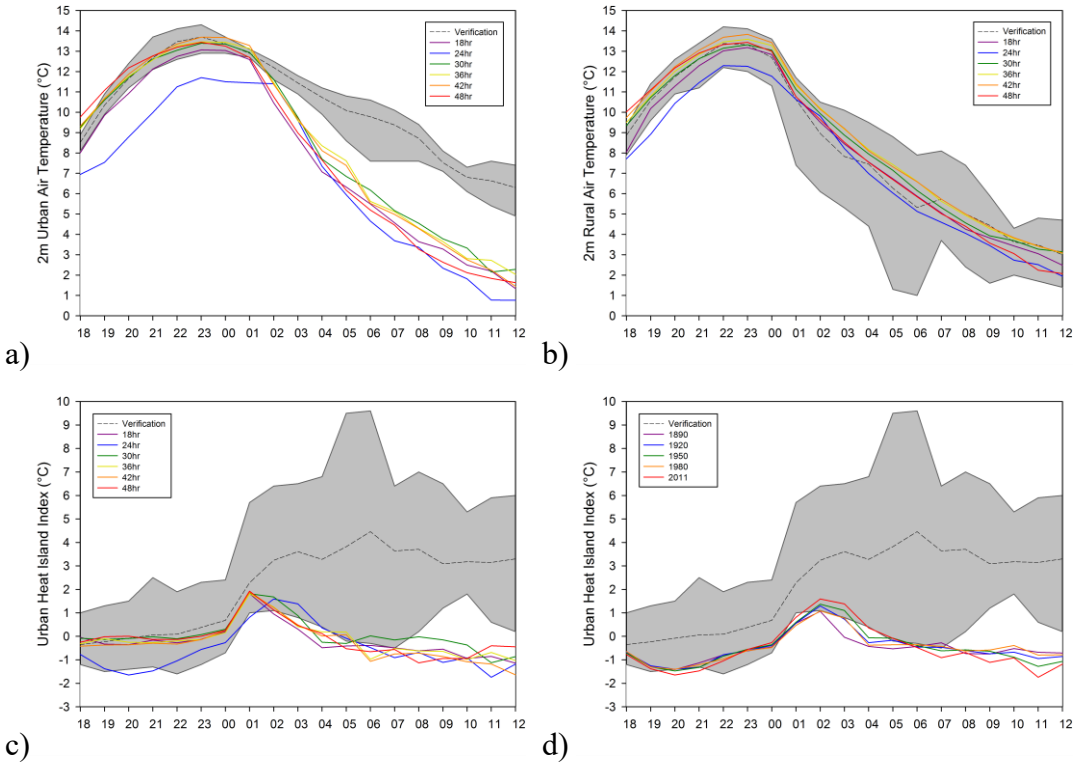

Figure 20. Run time accuracy of air temperature simulations at 2 m for urban stations (a), rural stations (b), and the resulting UHII (c) for 15 March 2009 case study. The simulation comparison of historical 24 hour UHII simulations (d) are also shown.

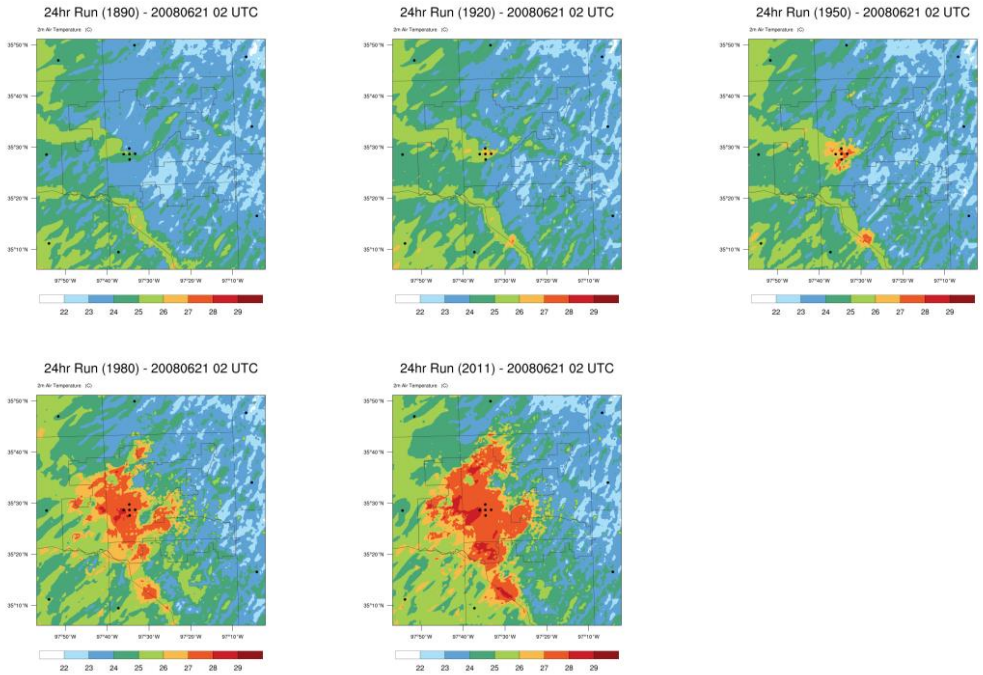

Figure 21. Air temperature at 2 m at 02 UTC from 1890, 1920, 1950, 1980, and 2011 for the 21 June 2008 case study.

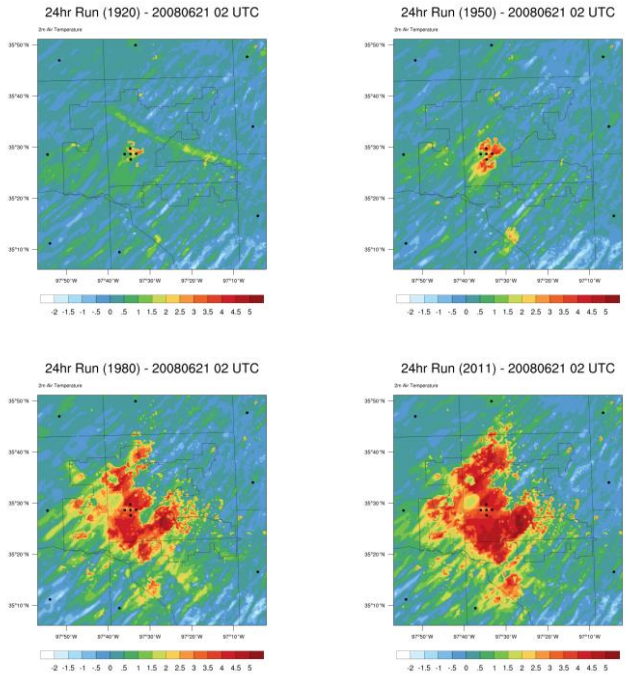

Figure 22. Air temperature difference at 2 m at 02 UTC from the 1890 land use model run for 1920, 1950, 1980, and 2011 for the 21 June 2008 case study.

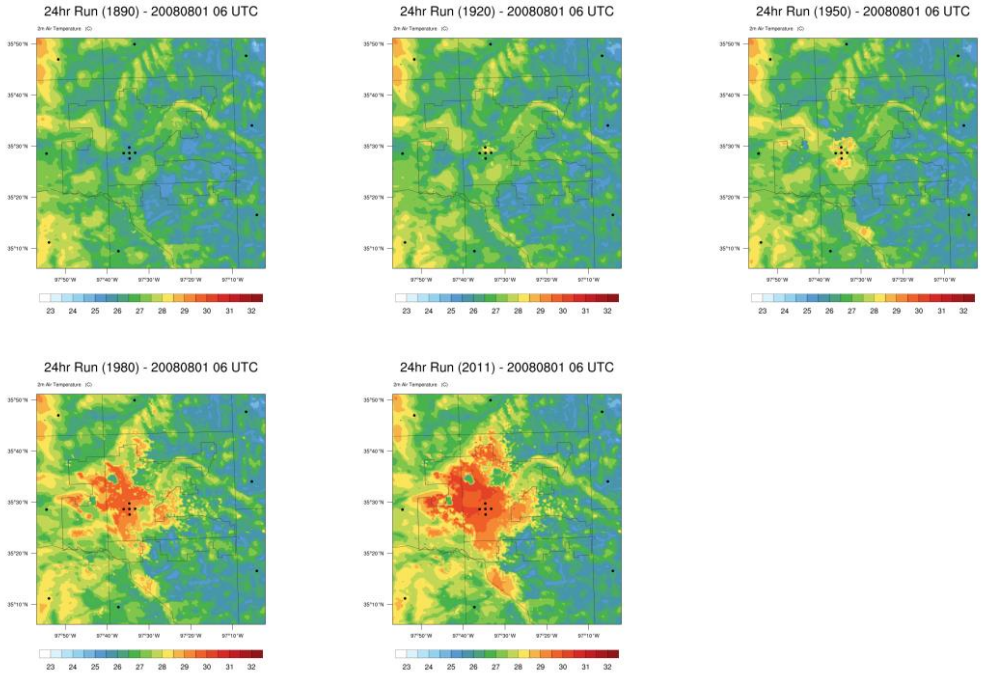

Figure 23. Air temperature at 2 m at 06 UTC from 1890, 1920, 1950, 1980, and 2011 for the 1 August 2008 case study.

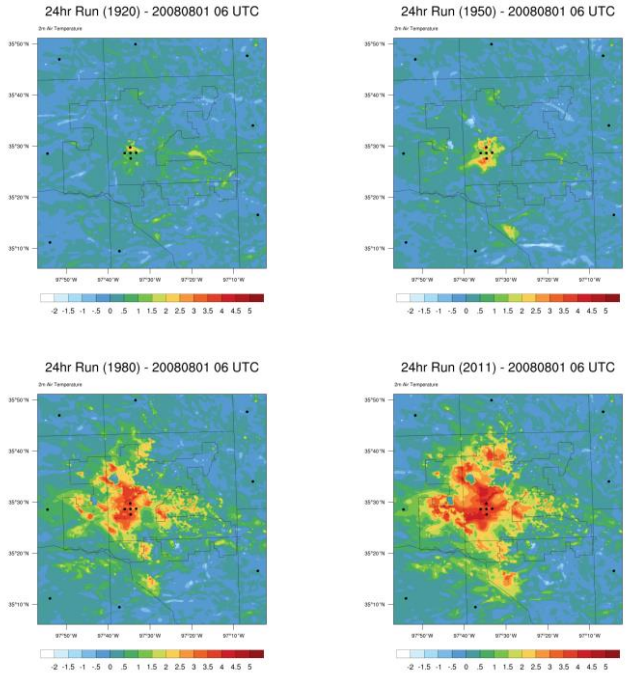

Figure 24. Air temperature difference at 2 m at 06 UTC from the 1890 land use model run for 1920, 1950, 1980, and 2011 for the 1 August 2008 case study.

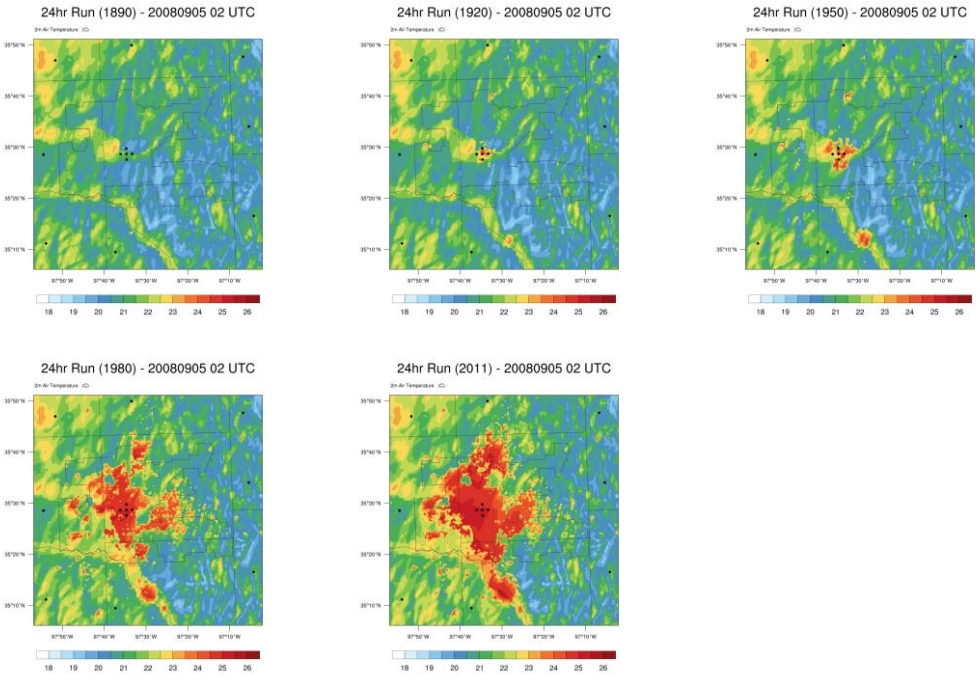

Figure 25. Air temperature at 2 m at 02 UTC from 1890, 1920, 1950, 1980, and 2011 for the 5 September 2008 case study.

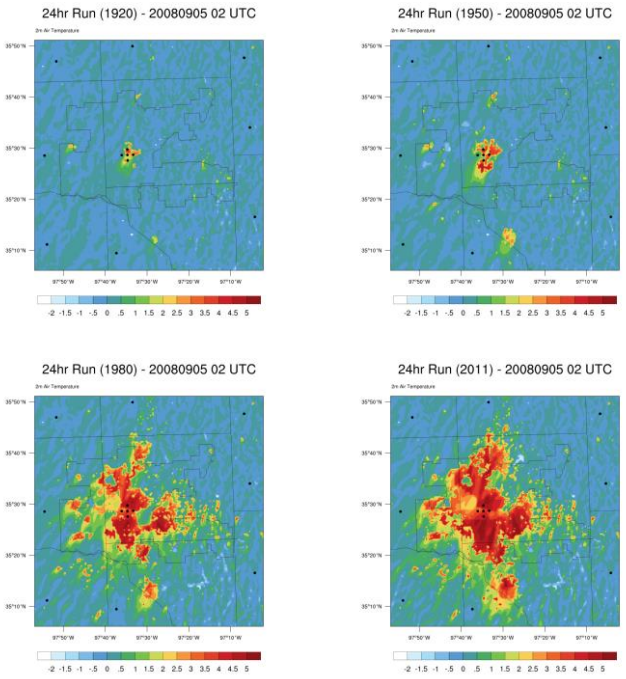

Figure 26. Air temperature difference at 2 m at 02 UTC from the 1890 land use model run for 1920, 1950, 1980, and 2011 for the 5 September 2008 case study.

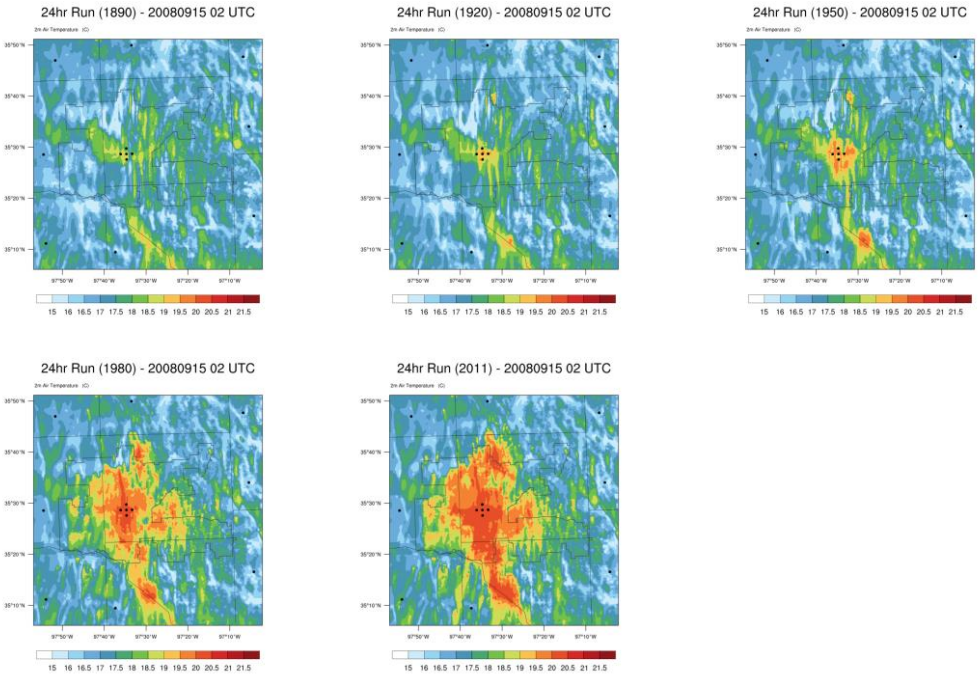

Figure 27. Air temperature at 2 m at 02 UTC from 1890, 1920, 1950, 1980, and 2011 for the 15 September 2008 case study.

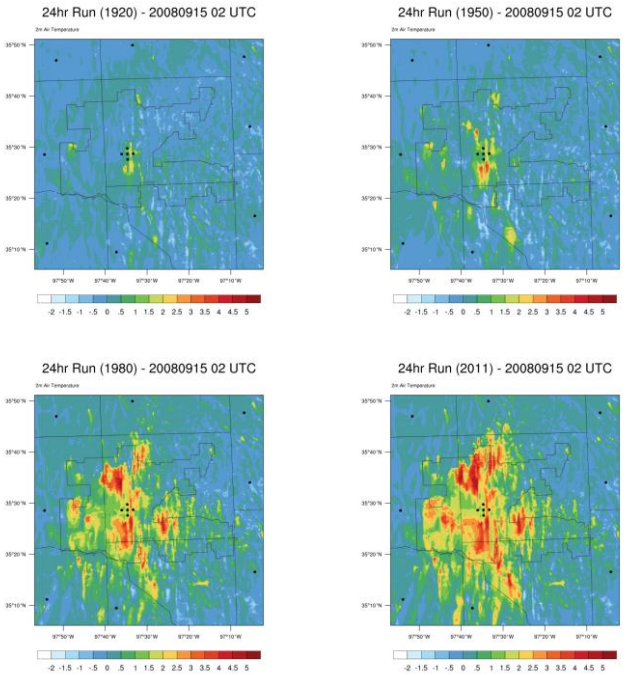

Figure 28. Air temperature difference at 2 m at 02 UTC from the 1890 land use model run for 1920, 1950, 1980, and 2011 for the 15 September 2008 case study.

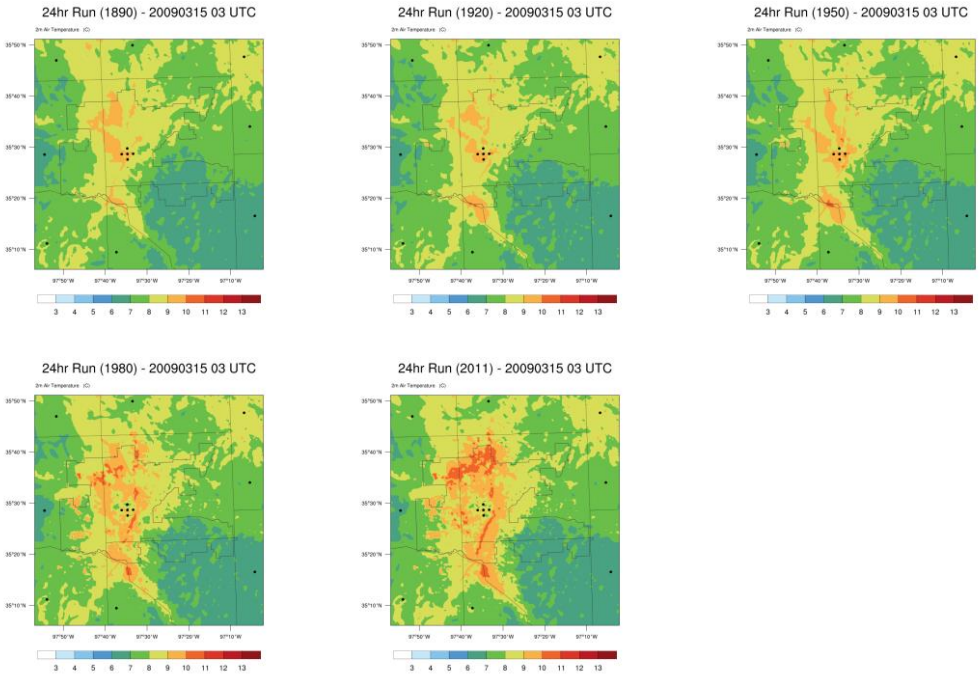

Figure 29. Air temperature at 2 m at 03 UTC from 1890, 1920, 1950, 1980, and 2011 for the 15 March 2009 case study.

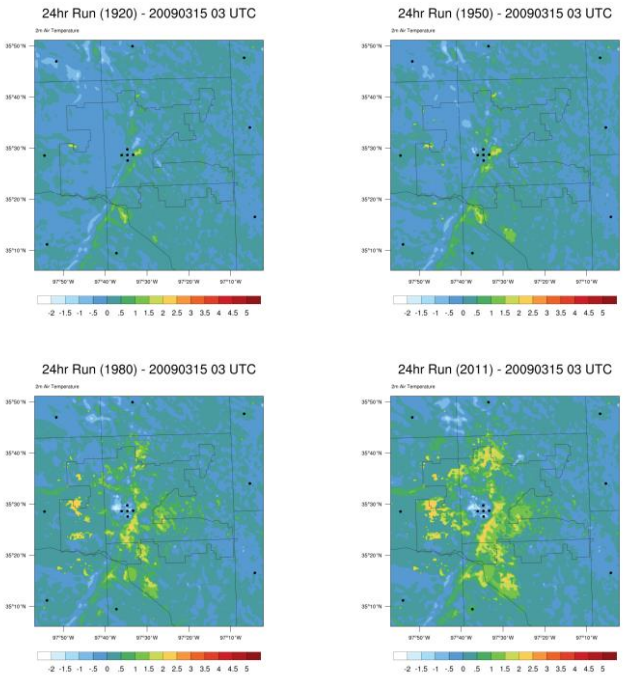

Figure 30. Air temperature difference at 2 m at 03 UTC from the 1890 land use model run for 1920, 1950, 1980, and 2011 for the 15 March 2009 case study.

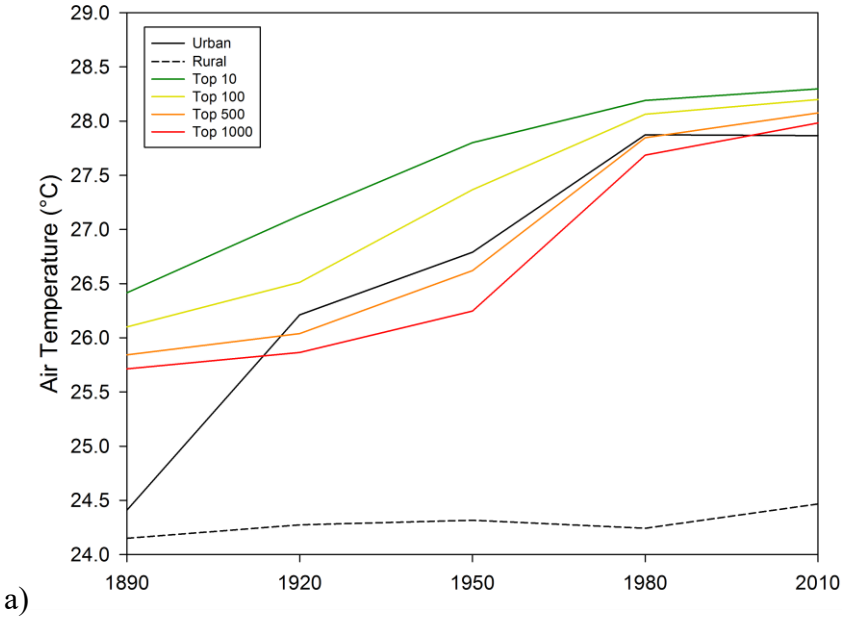

a)

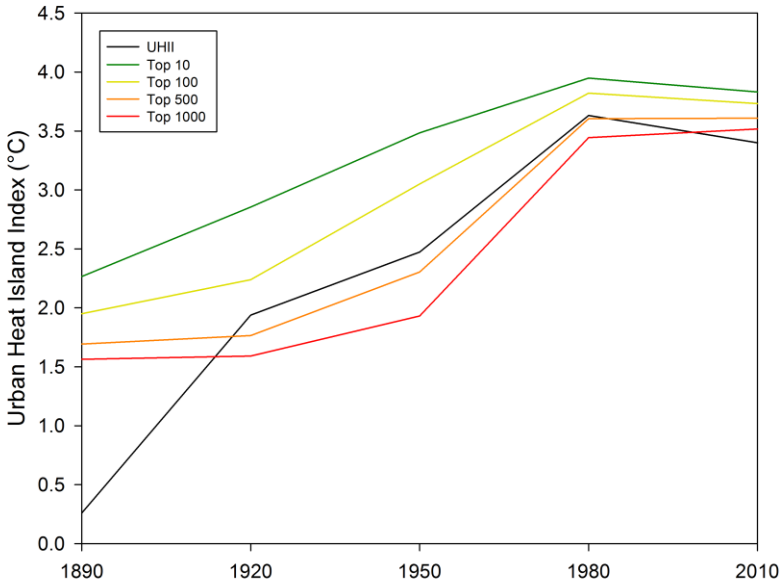

b)

Figure 31. Urban and rural air temperatures (a; "Urban", "Rural") and Urban heat island indices (b; "UHII") for arbitrary locations for the top 10, 100, 500, and 1000 warmest grid box locations in the 21 June 2008 at 02 UTC case study.

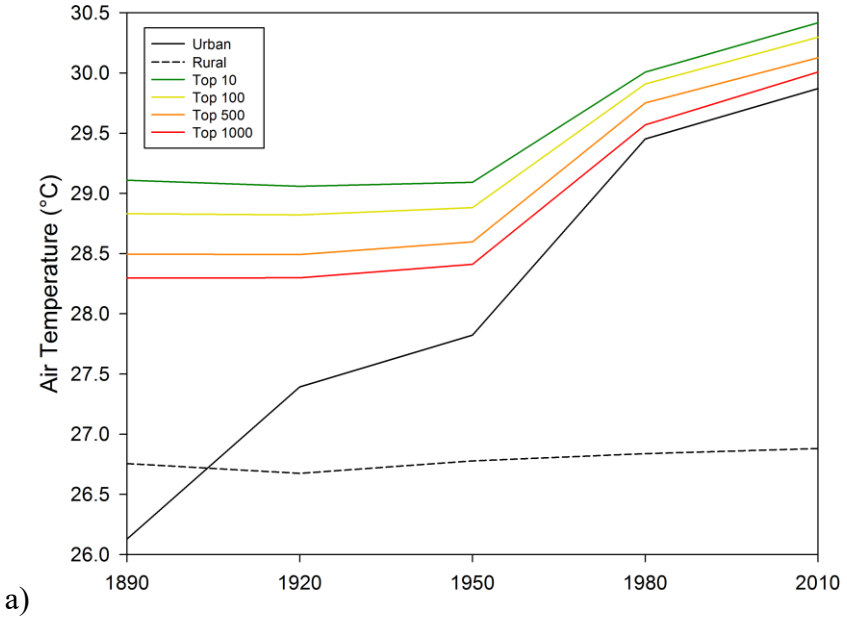

a)

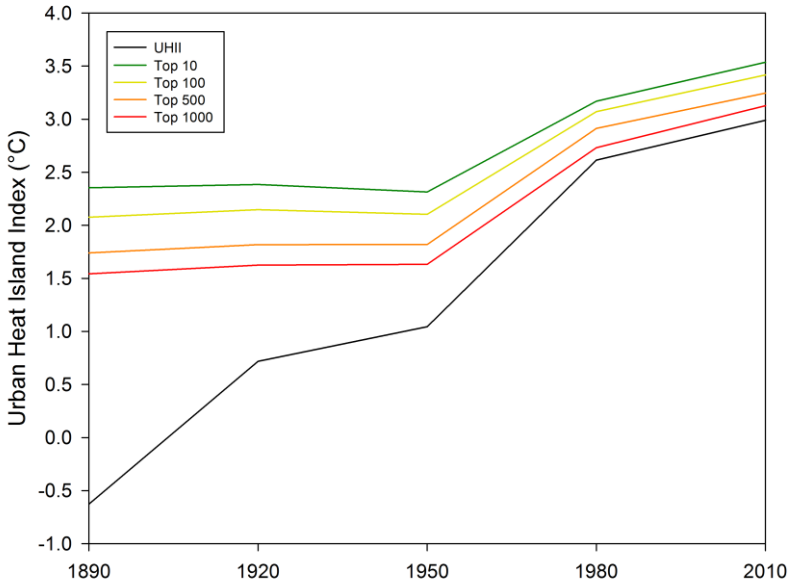

b)

Figure 32. Urban and rural air temperatures (a; “Urban”, “Rural”) and Urban heat island indices (b; “UHII”) for arbitrary locations for the top 10, 100, 500, and 1000 warmest grid box locations in the 1 August 2008 at 06 UTC case study.

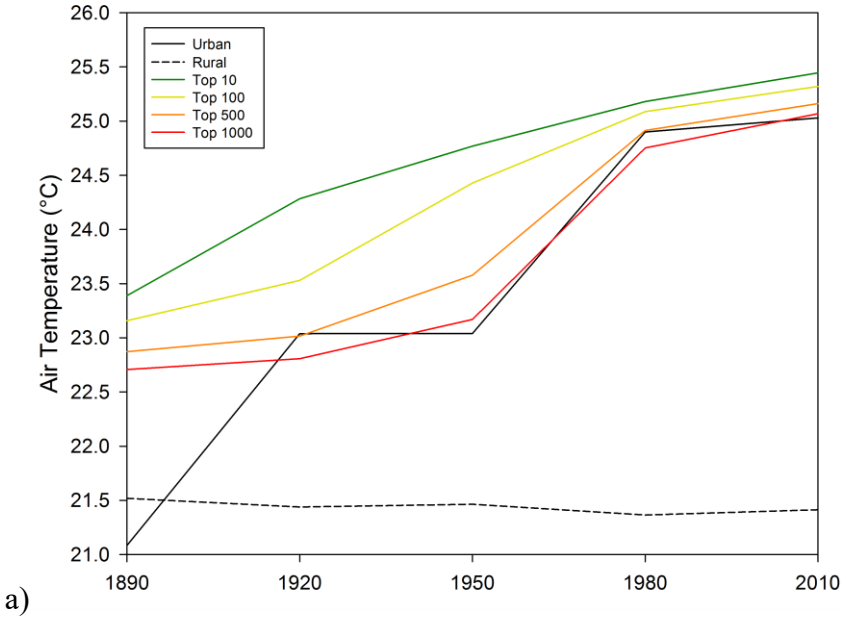

a)

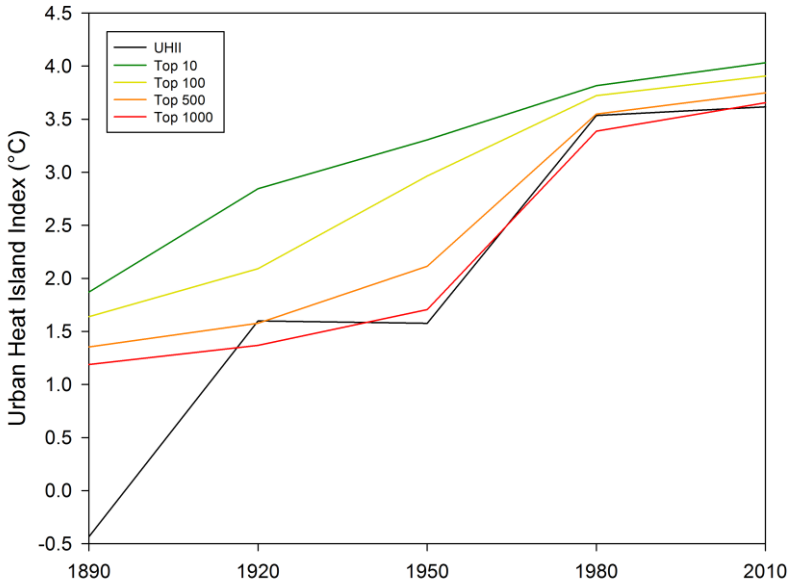

b)

Figure 33. Urban and rural air temperatures (a; “Urban”, “Rural”) and Urban heat island indices (b; “UHII”) for arbitrary locations for the top 10, 100, 500, and 1000 warmest grid box locations in the 5 September 2008 at 02 UTC case study.

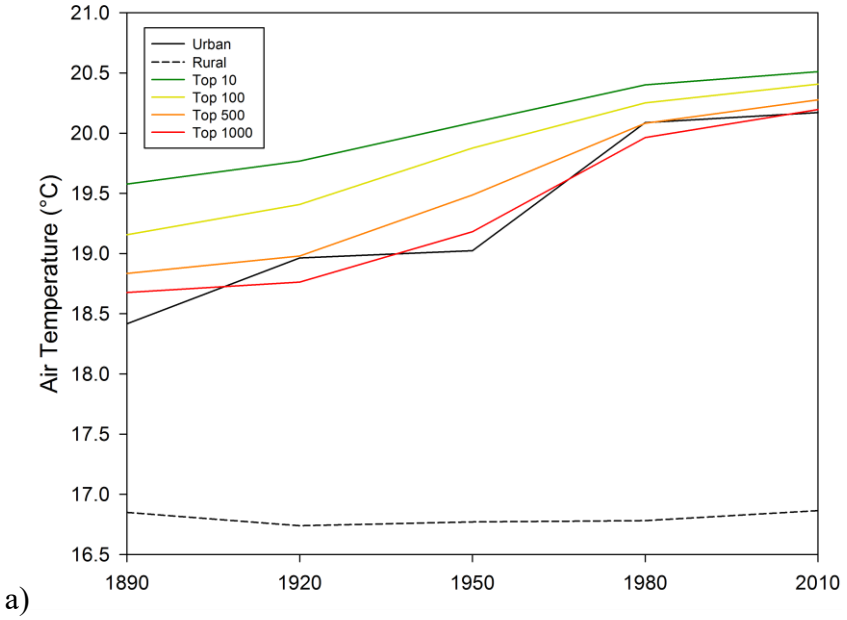

a)

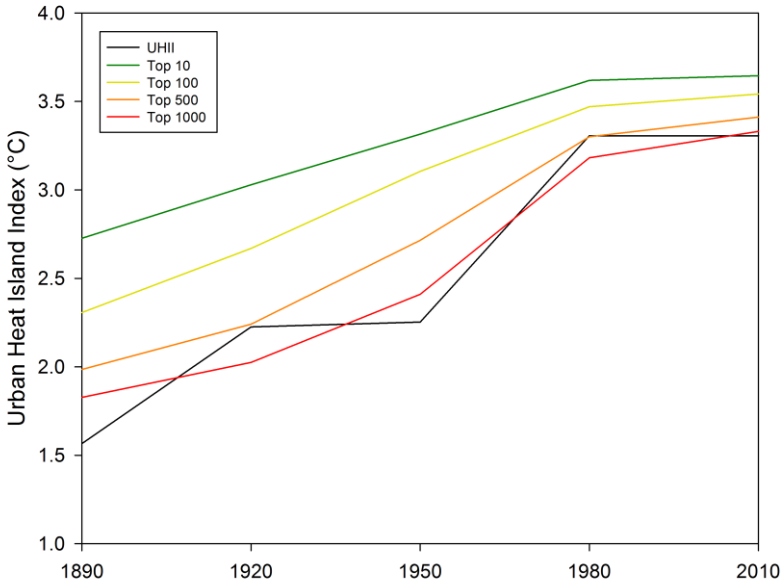

b)

Figure 34. Urban and rural air temperatures (a; "Urban", "Rural") and Urban heat island indices (b; "UHII") for arbitrary locations for the top 10, 100, 500, and 1000 warmest grid box locations in the 15 September 2008 at 02 UTC case study.

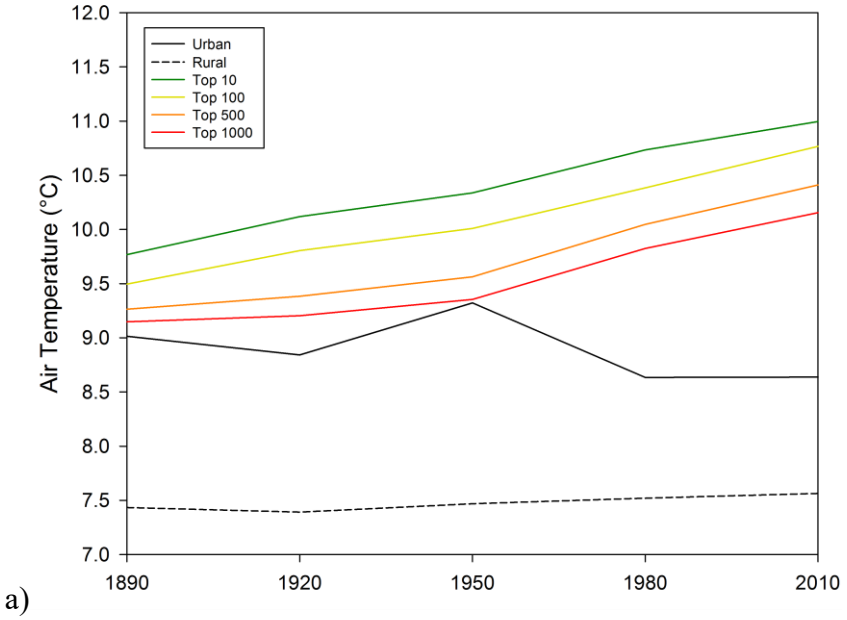

a)

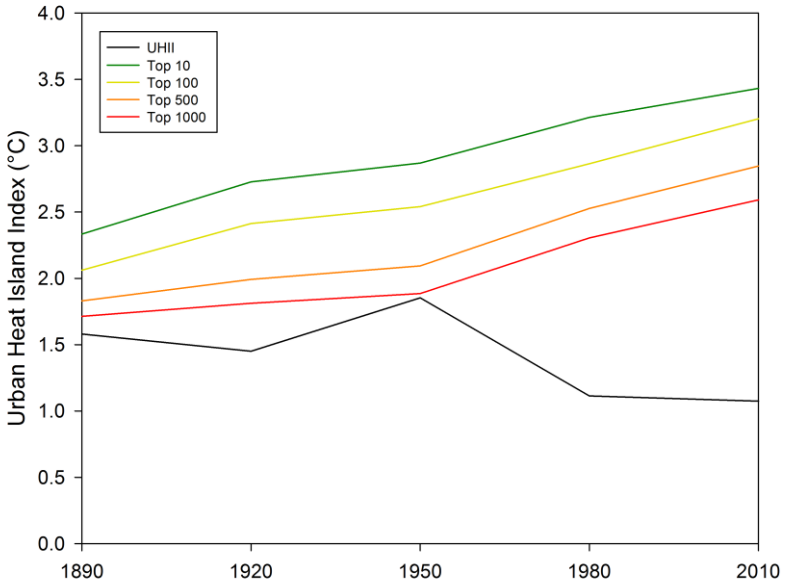

b)

Figure 35. Urban and rural air temperatures (a; "Urban", "Rural") and Urban heat island indices (b; "UHII") for arbitrary locations for the top 10, 100, 500, and 1000 warmest grid box locations in the 15 March 2009 at 03 UTC case study.

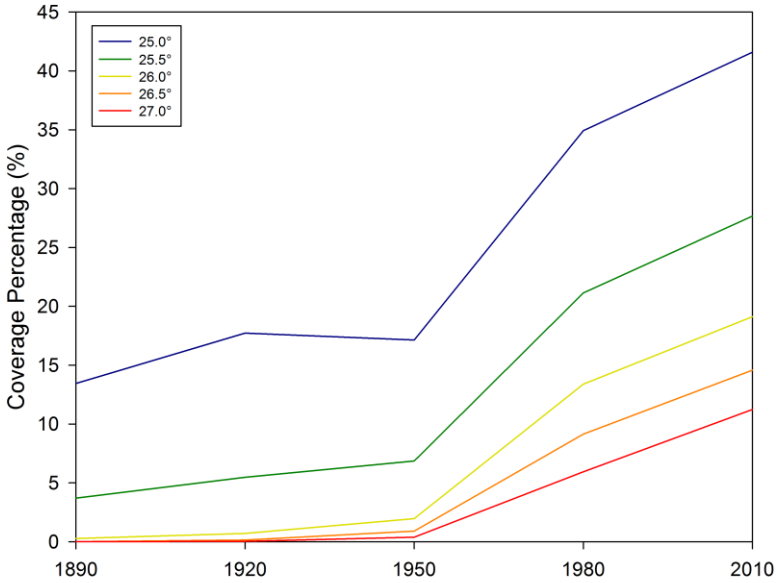

Figure 36. Air temperature coverage percentile increases in the 21 June 2008 at 02 UTC case study.

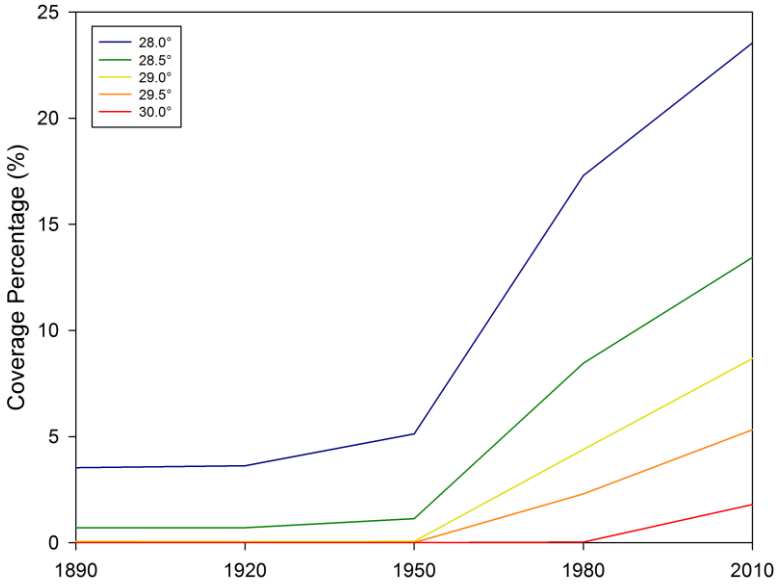

Figure 37. Air temperature coverage percentile increases in the 1 August 2008 at 03 UTC case study.

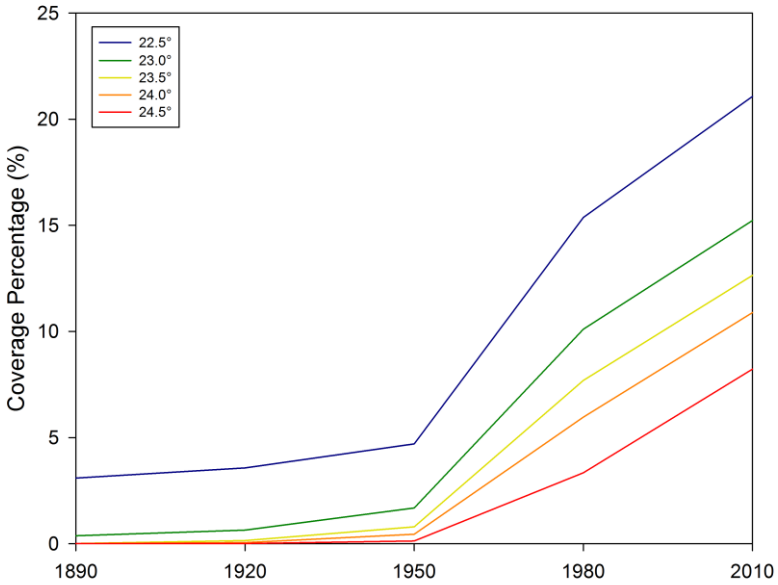

Figure 38. Air temperature coverage percentile increases in the 5 September 2008 at 02 UTC case study.

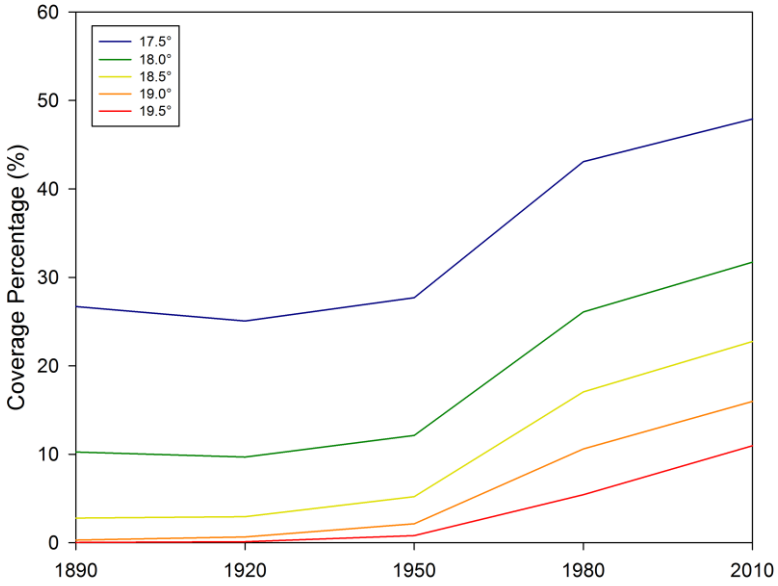

Figure 39. Air temperature coverage percentile increases in the 15 September 2008 at 02 UTC case study.

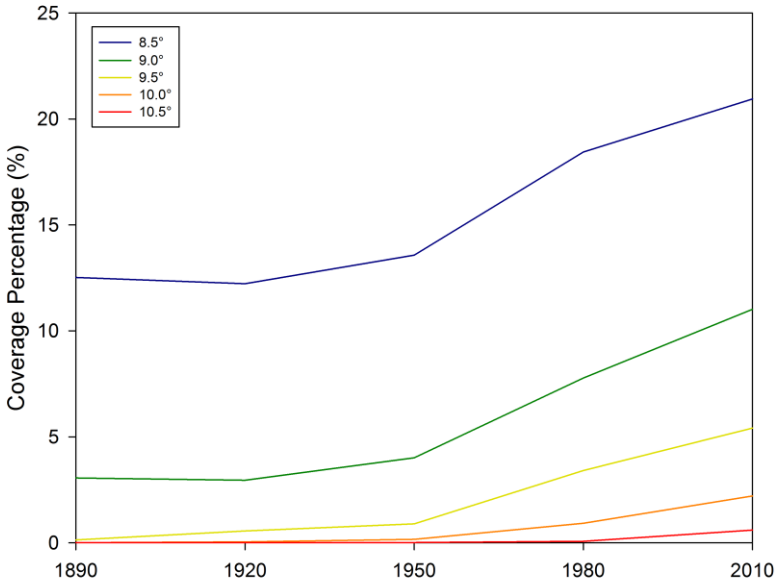

Figure 40. Air temperature coverage percentile increases in the 15 March 2009 at 03 UTC case study.

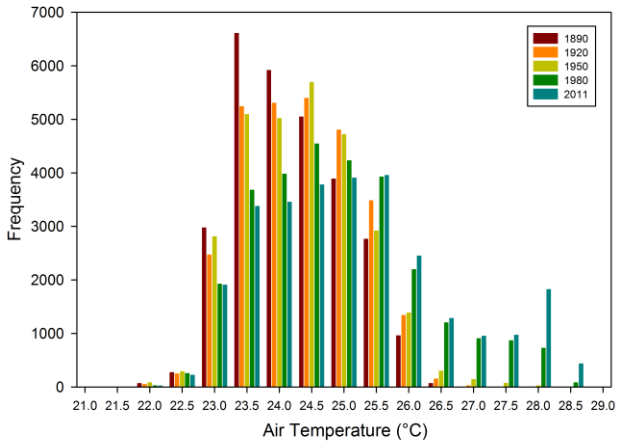

a)

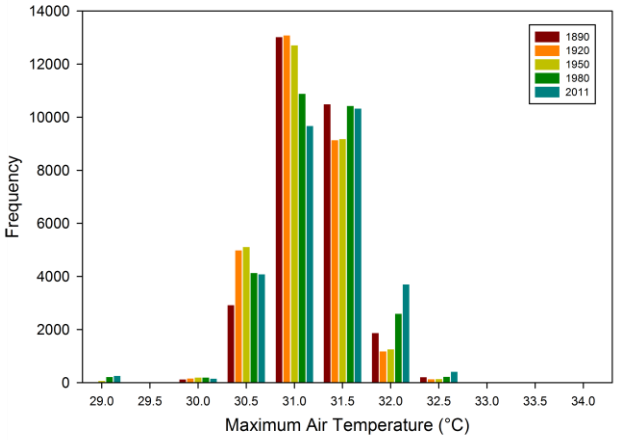

b)

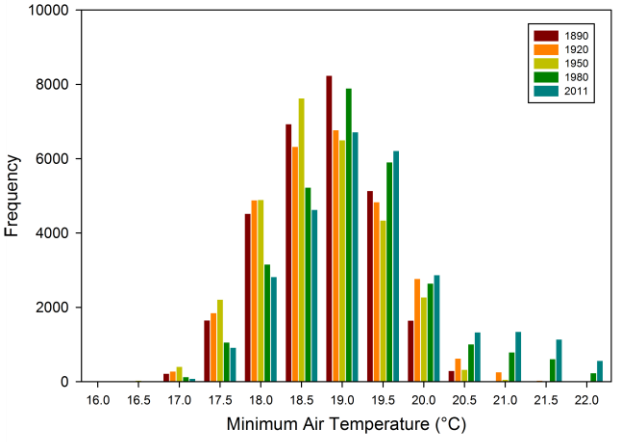

c)

Figure 41. Histogram of air temperatures at 2 m at 02 UTC (a), for the daily maximum (b), and for the daily minimum (c) for the 21 June 2008 case study.

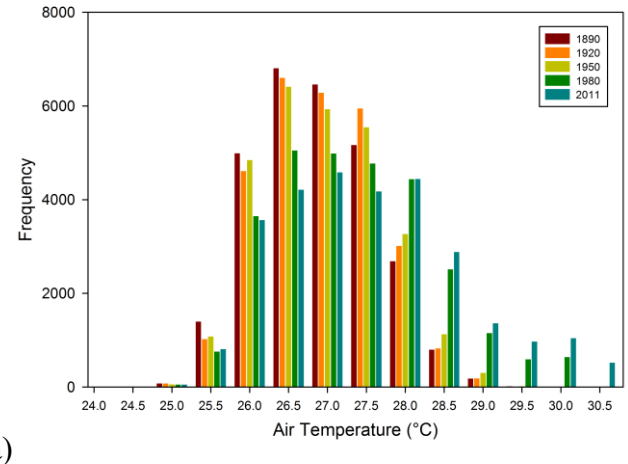

a)

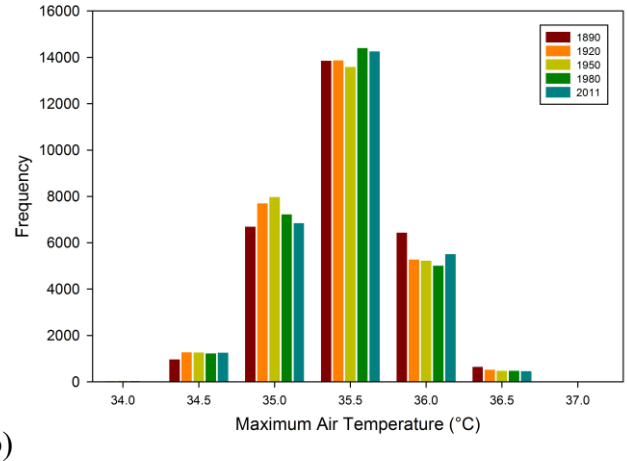

b)

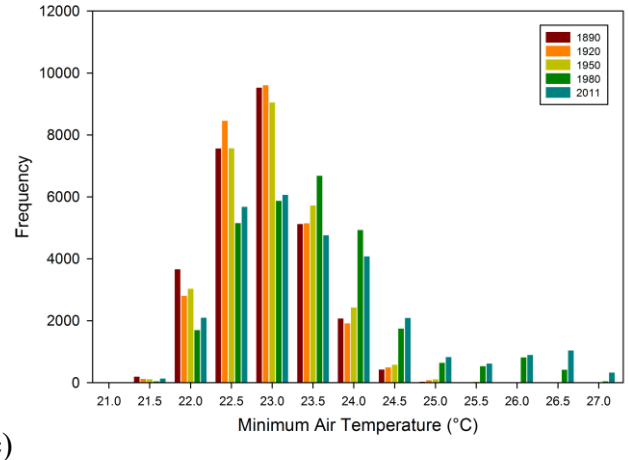

c)

Figure 42. Histogram of air temperatures at 2 m at 06 UTC (a), for the daily maximum (b), and for the daily minimum (c) for the 1 August 2008 case study.

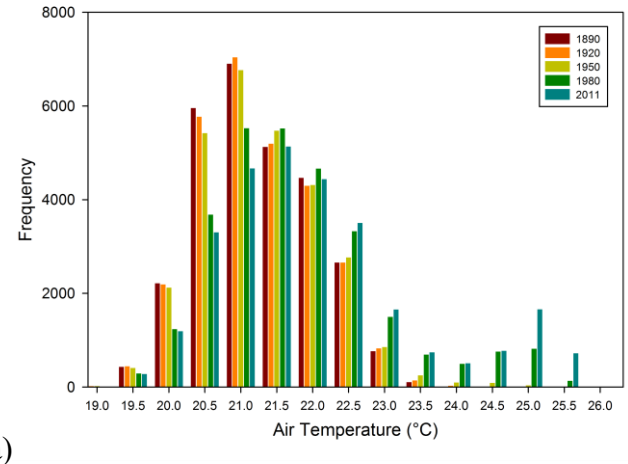

a)

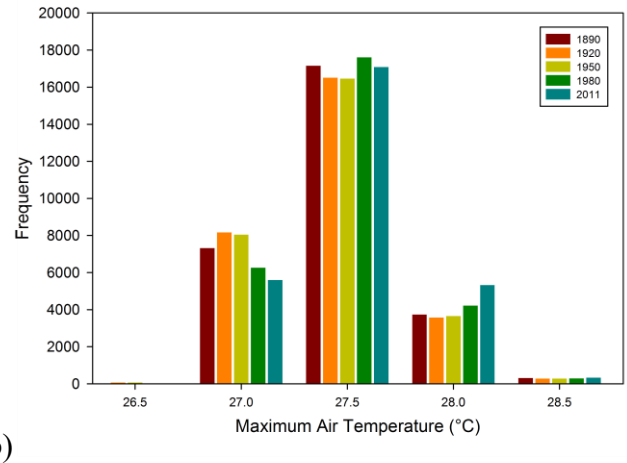

b)

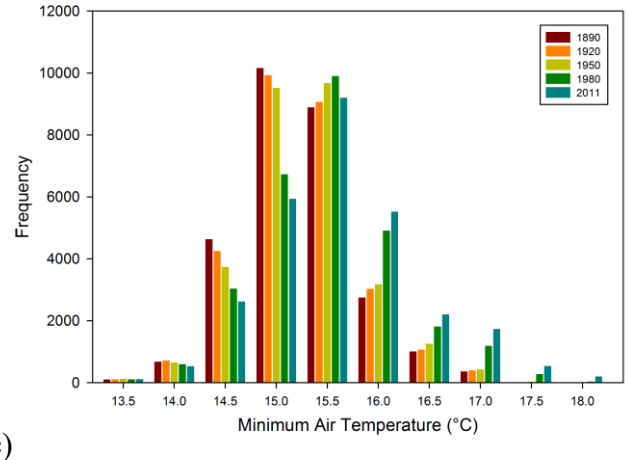

c)

Figure 43. Histogram of air temperatures at 2 m at 02 UTC (a), for the daily maximum (b), and for the daily minimum (c) for the 5 September 2008 case study.

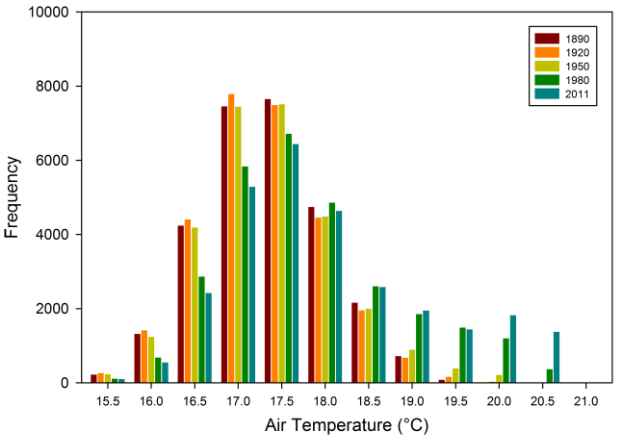

a)

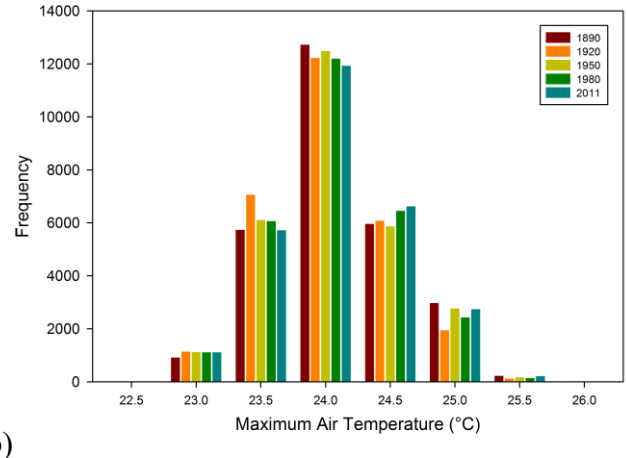

b)

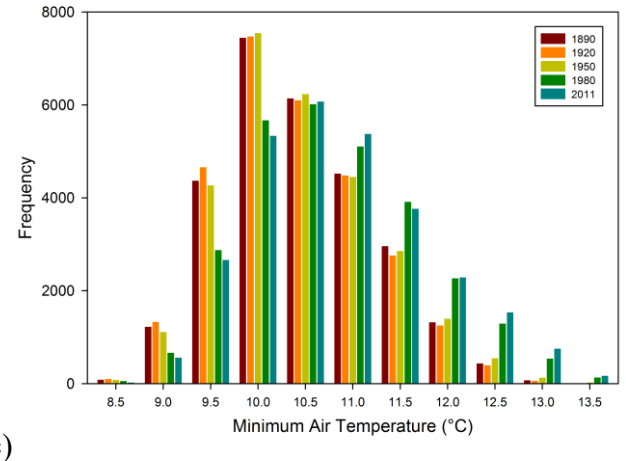

c)

Figure 44. Histogram of air temperatures at 2 m at 02 UTC (a), for the daily maximum (b), and for the daily minimum (c) for the 15 September 2008 case study.

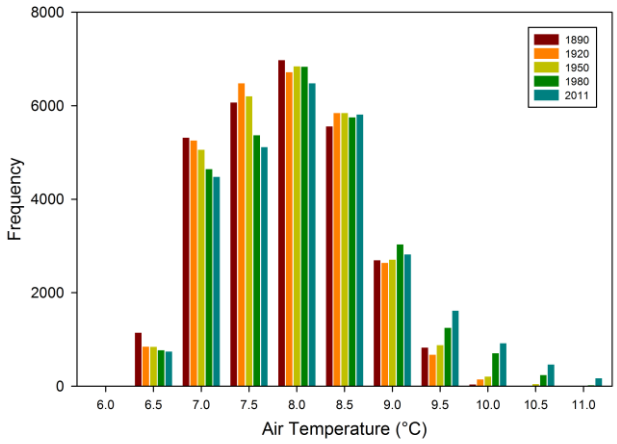

a)

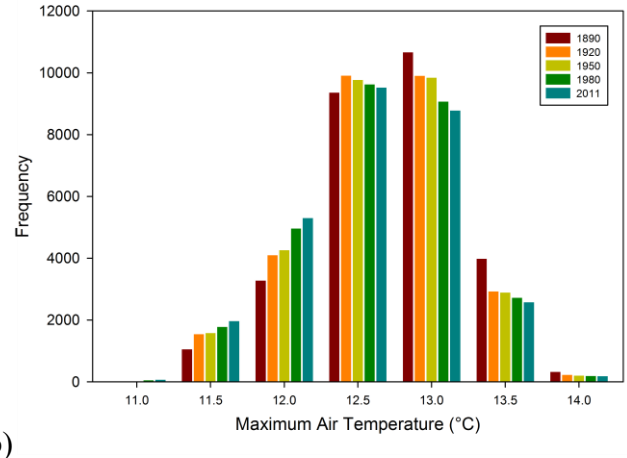

b)

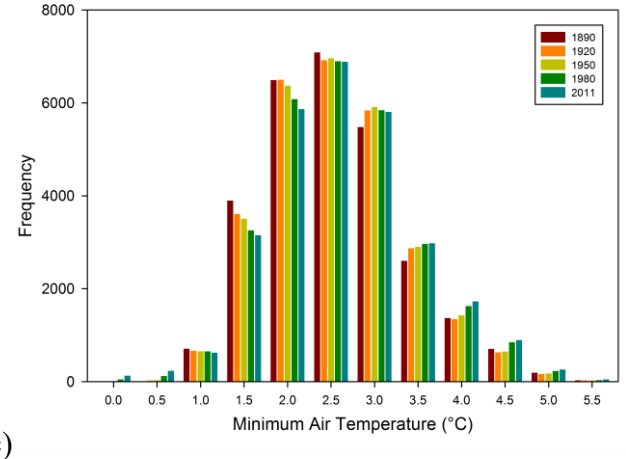

c)

Figure 45. Histogram of air temperatures at 2 m at 03 UTC (a), for the daily maximum (b), and for the daily minimum (c) for the 15 March 2009 case study.